EUCLIPSE

EU Cloud Intercomparison, Process Study & Evaluation Project

Grant agreement no. 244067

Deliverable D2.5:	Establish links between the representation of cloud and moist processes in ESMs and their ability to simulate the ITCZ, MJO and ENSO, and temperature extremes over Europe.
Delivery date:	54 months
Responsible partner:	MF-CNRM

EUCLIPSE WP2 Deliverable D2.5:

Report on the influence of the representation of cloud and moist processes in models on the simulation of the ITCZ, MJO, ENSO, and temperature extremes over Europe

Main contributors to this report:
Gilles Bellon, Julien Cattiaux, Hervé Douville, Boutheina Oueslati,
Deepa Raveendran Pillai, Romain Roehrig (CNRM, France)
Hugo Bellenger, Eric Guilyardi (LOCEAN/IPSL, France)
Traute Crueger, Benjamin Moebis, Bjorn Stevens (MPI-M, Germany)
Aiko Voigt (MPI-M, Germany and LMD/IPSL, France)
Sandrine Bony, Jean-Louis Dufresne, Solange Fermepin (LMD/IPSL, France)

July 2014 (Month 48)

WP2 is focused on the analysis and the evaluation of climate simulations from CMIP5 (the 5th Phase of the Coupled Models Intercomparison Project). An important component of WP2 is the analysis and understanding of the role that clouds and moist processes play in the present-day climate, especially in the general atmospheric circulation, natural climate variability, and temperature extremes over Europe. This activity turned out to be very cross-cutting across EUCLIPSE partners.

This deliverable reports on the role of clouds and moist processes in :

- *the Inter-Tropical Convergence Zone (ITCZ): structure, strength, shifts*
- *the Madden-Julian Oscillation (MJO)*
- *the El-Niño Southern Oscillation (ENSO)*
- *temperatures over Europe, including its extremes.*

These results are mostly based on the analysis of CMIP5 simulations. However, they are also based in part on additional simulations proposed and coordinated as part of EUCLIPSE WP4, in particular the so-called COOKIE experiments (Stevens et al. 2012), and on sensitivity studies performed with individual EUCLIPSE models.

Through these studies (which represent more than 16 publications, 10 being published already), EUCLIPSE has contributed to fundamental advances in our understanding and evaluation of the processes that control the dynamics and natural variability of the Earth's climate, and to a better understanding of uncertainties in temperature projections over Europe.

1 Influence of the representation of moist processes on the simulation of the ITCZ

1.1 On the role of convective entrainement in the structure of the ITCZ

The double ITCZ is still a strong bias in the CMIP5 coupled simulations. As measured by the Southern ITCZ (SI) index (Bellucci et al. 2010, annual mean precipitation between 100W and 150W, 20S and the equator), the CMIP5

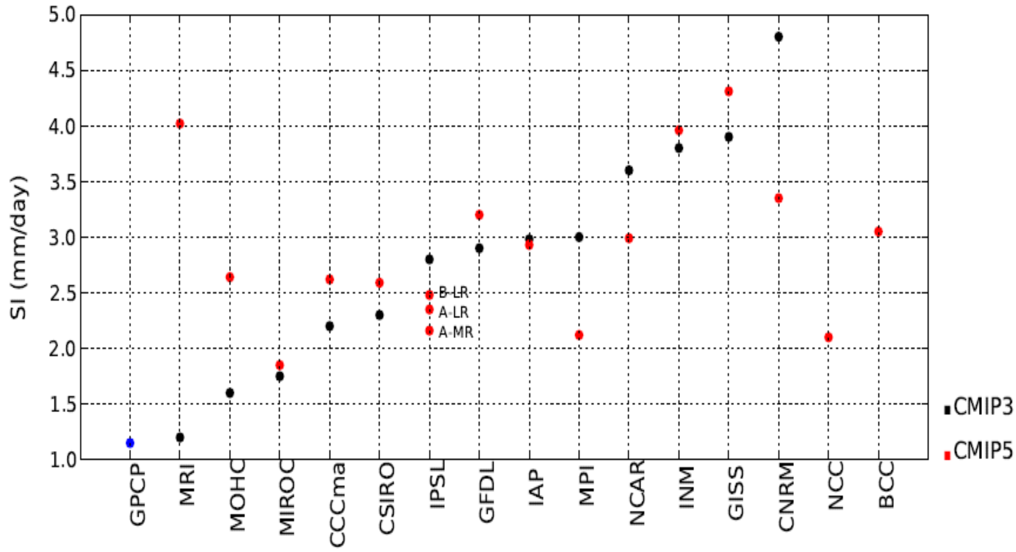

Figure 1: Southern ITCZ index in CMIP3 and CMIP5 coupled ocean-atmosphere simulations. The blue dot indicates the observations (GPCP).

models perform as well, or as poorly, as the CMIP3 models, as Figure 1 shows. As found in CMIP3 models, ocean-atmosphere coupling is a strong amplifier of the bias: atmosphere-only simulations yield a smaller double ITCZ bias than the coupled ocean-atmosphere simulations, as shown in Figure 2, except for one model (MIROC).

The main coupled ocean-atmosphere feedbacks that amplify this bias are well known (de Szoeke et al. 2008), and Bellucci et al. (2010) developed a metrics of the contribution of these feedbacks to the double ITCZ bias. We focused on the role of one moist process: the lateral entrainment in convective plumes. By mixing the cloudy air with environmental air, this entrainment reduces the humidity and buoyancy of the cloud and makes convection shallower and less frequent.

In the CNRM-CM5 model:

In the CNRM-CM5, convective entrainment can be controlled by a single parameter ε. In a series of sensitivity experiments, this parameter ε was arbitrarily halved or doubled (quintupled in the case of the coupled simulation). In the CNRM-CM5, the double ITCZ bias is present mostly in summer, it is reduced when the entrainment is increased both in atmosphere-only and coupled ocean-atmosphere simulations, as shown in Figure 3.

Indeed, it can be seen that the improvement of the simulation of the ITCZ in the central and eastern tropical Pacific comes at the expense of the simulation of the precipitation at the center of tropical convergence zones (over the West Pacific Warm Pool in boreal summer), that is significantly overestimated.

Changes in the humidity stratification are associated with this changes in the convection: increasing the entrainment dries the free troposphere, moistens the boundary layer in tropical convergence zones, and deepens the boundary layer in the subtropics. These results are consistent with those from aquaplanet simulations.

To better understand this sensitivity, the changes in circulation between the simulation with increased entrainment and that with reduced entrainment were studied. It was found that the PDF of the monthy vertical speed ω at 500 hPa transitions from a unimodal distribution with a maximum in weak subsidence to a bimodal distribution with maxima in weak subsidence and weak ascent when the entrainment is decreased, as can be seen in Figure 4 for both the atmosphere-only and aquaplanet simulations.

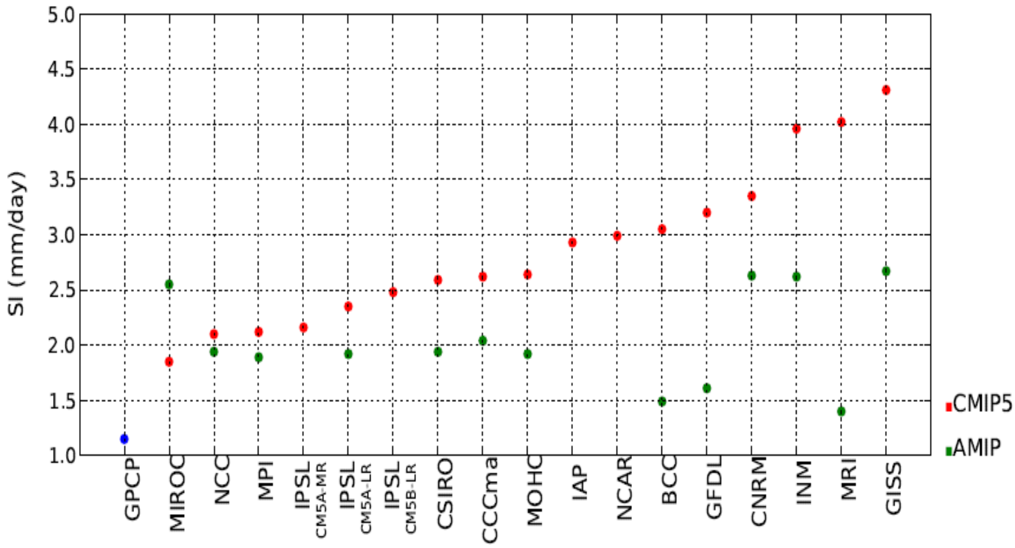

Figure 2: Southern ITCZ index in CMIP5 coupled ocean-atmosphere simulations and atmosphere-only simulations ("AMIP" simulations). The blue dot indicates the observations (GPCP).

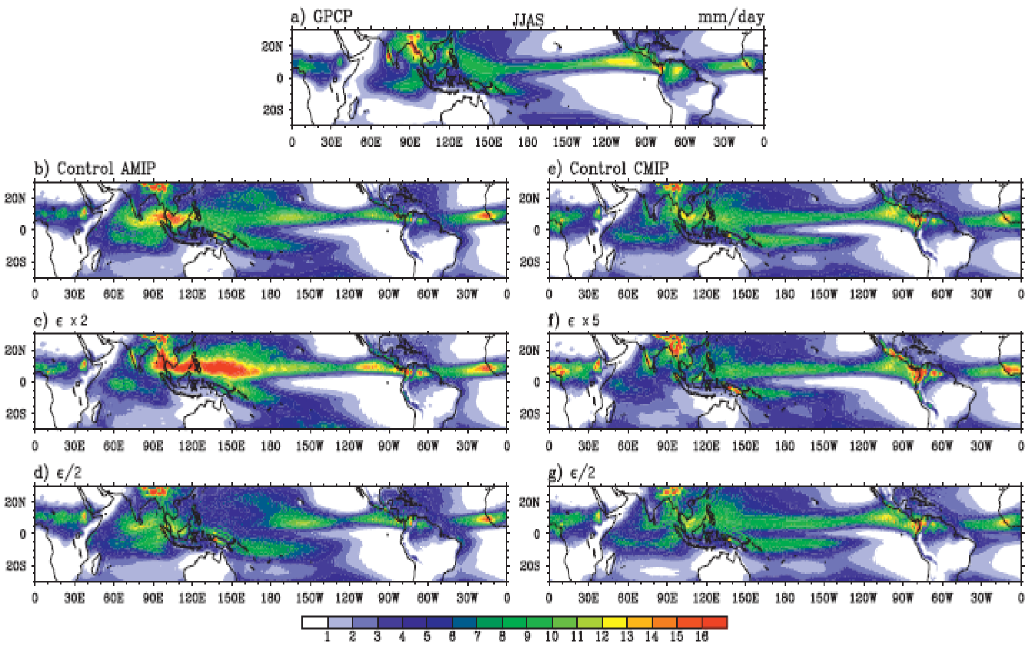

Figure 3: Present-day (1979-1999) July-to-September (JJAS) average precipitation (in mm/day) in the observations (GPCP, top) and in the CNRM atmosphere-only (AMIP) and coupled (CMIP) simulations, for different values of the entrainment parameter ε.

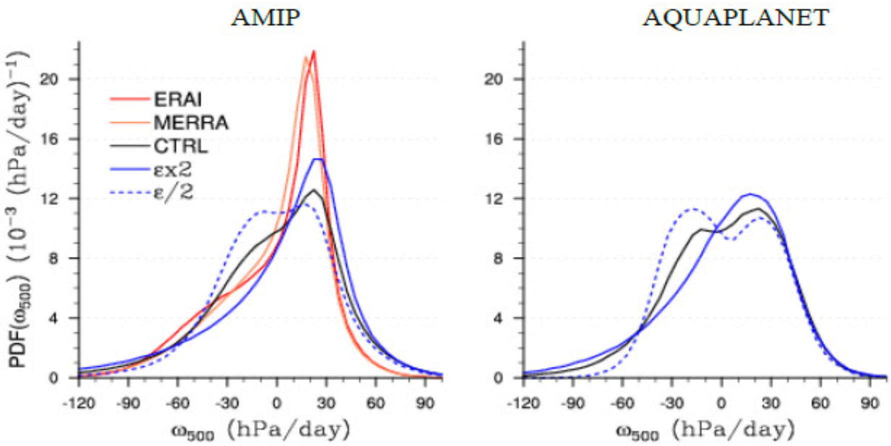

Figure 4: PDF of ω at 500 hPa in the tropics (30S-30N) in the reanalyses, atmosphere-only (left) ("AMIP") and (right) aquaplanet simulations for different values of the entrainment parameter ε.

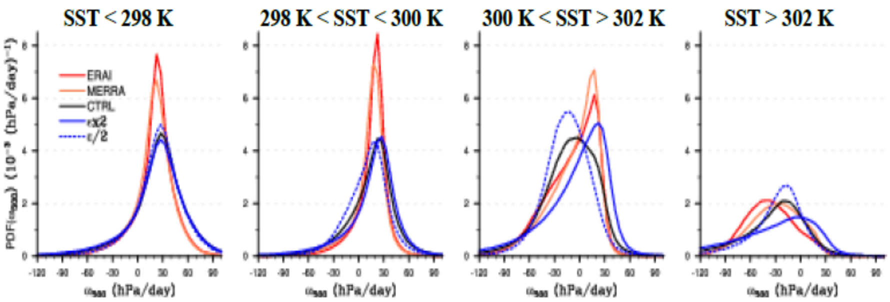

Figure 5: Contributions of the different SST ranges to the PDF of tropical ω at 500 hPa. From left to right: SST $<$ 298 K, 298 K $<$ SST $<$ 300 K, 300 K $<$ SST $<$ 302 K and SST $>$ 302 K.

Further analysis shows the same transition in the PDF of the monthly precipitation and in the PDF of vertically-integrated convective heating, which strongly suggests that this transition is due to the change in the modeled interaction between deep convection and circulation. These results are published in Oueslati and Bellon (2013).

Stratifying this PDF by SST ranges sheds some light on the reason behind this transition. Figure5 show the contribution of 2-K SST ranges to the total PDF of ω.

These contributions show that the bimodality of the low-entrainment PDF results from:

- a low threshold of sea-surface temperature for the transition from shallow to deep convection, from subsidence to ascent compared to the large-entrainment simulation.
- a preferred regime of ascent/precipitation over warm SST, with a low sensitivity to the SST and little variability beyond the synoptic scale (not shown), while there is no preferred ascending regime in the large-entrainment simulation, the most likely state being neutral (and less likely than the most-likely regime in the reduced-entrainment simulation) over warm SST.

These results are the subject of an article in preparation.

Based on this work, a metrics of the misrepresentation of the interaction between circulation and deep convection was proposed: it measures the quadratic error on the function that describes the contribution of each regime of vertical speed ω to the total precipitation in the tropics. This metrics was shown to provide information on the SI index that is independent and complementary to the ocean-atmosphere coupling metrics provided by Bellucci et al. (2010). These results are the subject of an article under review (Oueslati and Bellon, 2015).

In the MPI-ECHAM model:

Aqua planet experiments performed with fixed sea surface temperatures (SST) using the ECHAM6 GCM were studied to understand properties that influence the position of the ITCZ (Moebis and Stevens 2012). A single ITCZ develops when using the Nordeng scheme and a double ITCZ when using the Tiedtke scheme. The position of the ITCZ was found to depend on a feedback loop process wherein convective heating drives pressure gradients and winds, which determine the rate of surface evaporation, which influences the boundary layer moist static energy, which finally couples back to the pattern of convective heating. This feedback loop process is sensitive to the SST profile and the choice of the convection scheme. However SSTs are only important in so far as they control the boundary layer moist static energy. The feed-back loop can be broken by specifying the wind used to calculate surface fluxes, in so doing it is possible to control the magnitude of boundary layer moist static energy and hence the position of the ITCZ. The cloud top height and therefore the convective heating decisively depends on the entrainment rates and the free tropospheric humidity. In the double ITCZ case the humidity in the lower free troposphere is higher on the equatorward side of the double ITCZ compared to the poleward side. Therefore an increase of the entrainment rates favor convection on the equatorward side. This explains why the Nordeng scheme produces a single ITCZ, although the Tiedtke scheme produces a double ITCZ.

References:

- Bellon, G., and B. Oueslati, 2015: Understanding the CNRM-CM5 sensitivity to convective entrainment, *Clim. Dyn.*, in preparation.
- Bellucci, A., S. Gualdi, A. Navarra, 2010: The Double-ITCZ Syndrome in Coupled General Circulation Models: The Role of Large-Scale Vertical Circulation Regimes. *J. Climate*, 23, 11271145.
- Moebis, B., and B. Stevens, 2012: Factors controlling the position of the Intertropical Convergence Zone on an aquaplanet, *J. Adv. Model. Earth Syst.*, **4**, M00A04, doi:10.1029/2012MS000199.
- Oueslati, B., and G. Bellon, 2013: Convective entrainment and large-scale organization of tropical precipitation: sensitivity of the CNRM-CM5 hierarchy of models, Journal of Climate,**26**(9), 2931-2946, doi:10.1175/JCLI-D-12-00314.1.
- Oueslati, B., and G. Bellon, 2015: The double ITCZ bias in CMIP5 models: interaction between SST, large-scale circulation and precipitation, submitted to *Climate Dynamics*.
- de Szoeke, Simon P., Shang-Ping Xie, 2008: The Tropical Eastern Pacific Seasonal Cycle: Assessment of Errors and Mechanisms in IPCC AR4 Coupled OceanAtmosphere General Circulation Models. *J. Climate*, 21, 25732590.

1.2 Role of cloud radiative effects in the tropical circulation

Mean circulation and precipitation

The role of atmospheric cloud radiative effects (ACRE) in the atmospheric circulation and its response to specified perturbations was investigated through EUCLIPSE experiments (proposed in WP4, Stevens et al. 2012) in which clouds were assumed to be transparent to radiation.

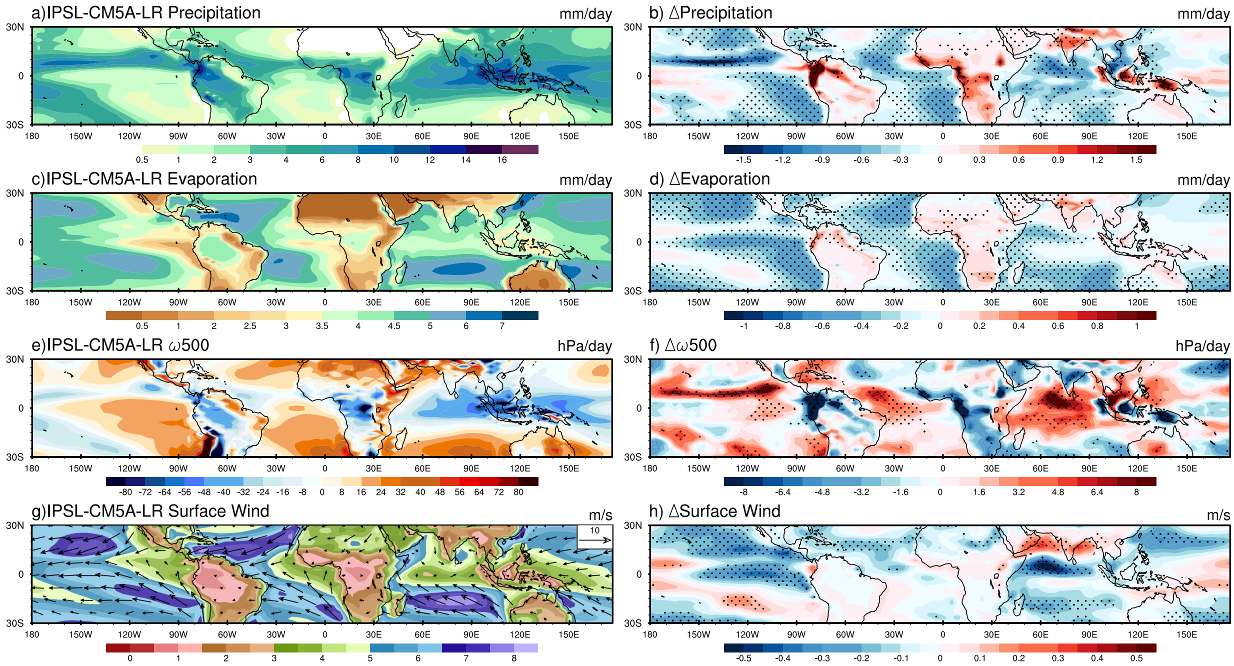

Figure 6: Annual mean change (offpblamip-amip difference averaged over 30 years) in tropical precipitation and circulation predicted by the IPSL-CM5A-LR model when boundary-layer clouds are made transparent to radiation: Control (left) and difference (right) of tropical precipitation (upper panels), 500hPa vertical velocity ($\omega500$, middle panels) and 10 meter wind (lower panels). Changes that are significant at the 95% level are stippled. [From Fermepin and Bony 2014]

Early studies using Atmospheric General Circulation Models (AGCMs) have shown that the ACRE exerts a strong influence on convection, precipitation and the general atmospheric circulation. In those studies, the role of ACRE in the circulation was primarily related to the radiative heating effect of deep convective clouds which dominates the tropical ACRE. In comparison, the role of the radiative cooling exerted by low-level clouds within the planetary boundary-layer (PBL) has received much less attention. Yet, PBL clouds constitute the predominant cloud type over tropical oceans.

By using an atmospheric general circulation model (IPSL-CM5A-LR) in different configurations (AMIP, aqua-planet, Transpose-AMIP), we have investigated the role that this cloud radiative cooling plays in the present-day climate (Fermepin and Bony 2014). Consistently with Brient and Bony (2012), we found that the ACRE tends to increase the low-level cloud fraction, owing to a positive feedback between radiative effects, temperature and relative humidity. We also found that low-cloud radiative effects increase the tropics-wide precipitation, strengthen the winds at the surface of the tropical oceans, and amplify the overturning circulation (Fig 6). By analyzing the vertically-integrated water and energy budgets of the atmosphere, we show that most of these effects arises from the strong coupling of cloud-radiative cooling with turbulent fluxes (the sum of latent plus sensible heat flux) at the ocean surface.

Moreover, by carrying experiments in which the climate model is used in a Numerical Prediction Mode (Transpose-AMIP), we have shown that the impact of cloud-radiative effects on atmospheric dynamics and precipitation was occuring on very short timescales (within a few days). Therefore, short-term atmospheric forecasts constitute a valuable framework for evaluating the interactions between cloud processes and atmospheric dynamics, and for assessing their dependence on model physics.

Shifts of the Inter-Tropical Convergence Zone

Despite a substantial hemispheric asymmetry in clear-sky albedo, observations of Earth's radiation budget reveal that the two hemispheres have the same all-sky albedo. Here, aquaplanet simulations with the atmosphere general circulation model ECHAM6 coupled to a slab ocean are performed to study to what extent and by which mechanisms clouds compensate hemispheric asymmetries in clear-sky albedo (Voigt et al. 2014a).

Clouds adapt to compensate the imposed asymmetries because the intertropical convergence zone (ITCZ) shifts into the dark surface hemisphere. The strength of this tropical compensation mechanism is linked to the magnitude of the ITCZ shift. In some cases the ITCZ shift is so strong as to overcompensate the hemispheric asymmetry in clear-sky albedo, yielding a range of climates for which the hemisphere with lower clear-sky albedo has a higher all-sky albedo. The ITCZ shift is sensitive to the convection scheme and the depth of the slab ocean. Cloud-radiative feedbacks explain part of the sensitivity to the convection scheme as they amplify the ITCZ shift in the Tiedtke (TTT) scheme but have a neutral effect in the Nordeng (TNT) scheme. A shallower slab ocean depth, and thereby reduced thermal inertia of the underlying surface and increased seasonal cycle, stabilizes the ITCZ against annual-mean shifts. The results lend support to the idea that the climate system adjusts so as to minimize hemispheric albedo asymmetries, although there is no indication that the hemispheres must have exactly the same albedo.

In another study (Voigt et al. 2014b), we investigate the role of cloud-radiative effects in the latitudinal shifts of the ITCZ induced by hemispheric surface albedo forcings. The problem is approached using aquaplanet simulations run with four comprehensive atmosphere models coupled to a slab ocean model (two versions of the IPSL model, and two versions of the MPI model, the different versions differing only by their representation of cloud and convective processes).

Through an energetic analysis of the ITCZ shifts (including an analysis of the cross-equatorial energy transport), we show that the radiative impact of clouds on the ITCZ shift differed in sign and in magnitude across the different models, and is responsible for half of the model spread in the ITCZ shift. By comparing experiments with interactive clouds or "locked clouds" (i.e. in which clouds in the perturbed experiments are prescribed to their control value), we show that the model spread is dominated by the radiative impact of tropical clouds, and that whose radiative impact is linked to the dependence of their cloud radiative properties on the circulation. This study does not only demonstrate the importance of clouds for circulation changes but also propose a way to reduce the model uncertainty in ITCZ shifts.

References:

- Brient, F. and S. Bony, 2012: How may low-cloud radiative properties simulated in the current climate influence low-cloud feedbacks under global warming? *Geophys. Res. Lett.*, **39**, L20807, doi:10.1029/2012GL053265.

- Fermepin S. and S. Bony, 2014: Influence of low-cloud radiative effects on tropical circulation and precipitation. *J. Adv. Model. Earth Syst.*, in press.

- Stevens B., S. Bony and M. Webb, 2012: Clouds On-Off Klimate Intercomparison Experiment (COOKIE). Available on `http://www.euclipse.eu/downloads/Cookie.pdf`.

- Voigt, A., B. Stevens, J. Bader, and T. Mauritsen, 2014a: Compensation of hemispheric albedo asymmetries by shifts of the ITCZ and tropical clouds, *J. Climate*, 27, 1029–1045, doi: http://dx.doi.org/10.1175/JCLI-D-13-00205.1

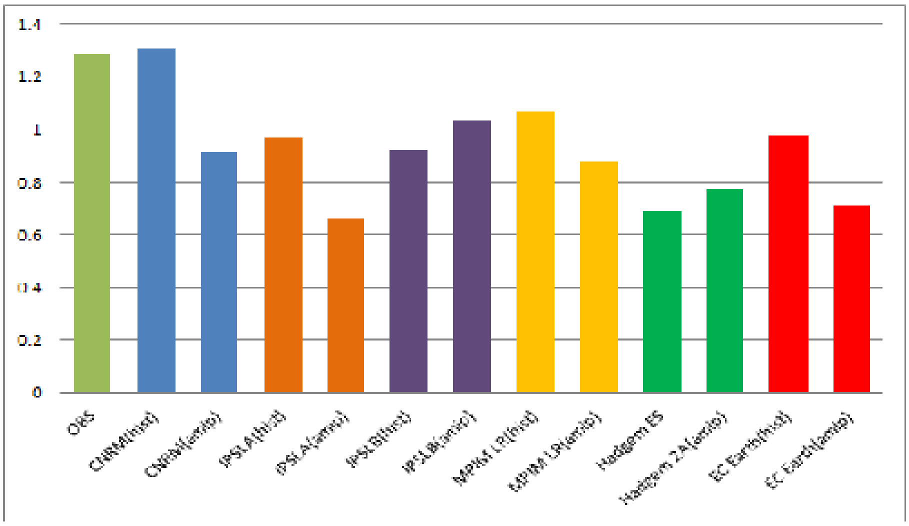

Figure 7: Ratio of the power of eastward propagating v.s. westward propagating disturbances in observations (OLR from NOAA), and in CMIP5 coupled ocean-atmosphere and atmosphere-only ("AMIP") simulations (adapted from Hung et al. 2013).

- Voigt, A., S. Bony, J.-L. Dufresne, and B. Stevens, 2014b : The radiative impact of clouds on the shift of the inter-tropical convergence zone. *Geophys. Res. Lett.*, in press.

2 Influence of the representation of moist processes on the simulation of the MJO

The simulation of the Madden-Julian Oscillation is still a challenge for the CMIP5 models. Figure 7 shows a classical metrics of the simulation of the MJO (the ratio between easward and westward propagation, E/W ratio), that shows that most coupled models still struggle to simulate more eastward than westward propagation. The CNRM model is an exception in its coupled version. Also, Figure 7 shows that ocean-atmosphere coupling has a positive impact on the MJO simulation in most models, but there are a significant number of models (two out of 6) that show a deterioration of the MJO simulation with ocean-atmosphere coupling. Note that these two models exhibit the lowest E/W ratios among coupled models.

Besides their impact on the atmosphere circulation through condensation-evaporation diabatic processes, clouds have a strong radiative contribution to the energy budgets of the atmosphere and ocean, and participate to ocean-atmosphere coupled mechanisms. Despite a few studies suggesting a significant role of radiative processes in the MJO (Raymond 2001, Bony and Emanuel 2005), they have received little attention.

To investigate this role, especially within CMIP5 models, two main studies were carried out as part of EUCLIPSE: (1) an analysis of CMIP5 model outputs focusing on the radiative budget of intraseasonal variability in the eastern equatorial Indian Ocean (75E-100E, 10S-10N), and (2) an analysis of EUCLIPSE-coordinated experiments in which cloud-radiative effects are switched off (refered to as COOKIE experiments, Stevens et al. 2012)

2.1 Radiative budget of intraseasonal variability in CMIP5 models

The variables of interest are spatially-averaged over this region and their intraseasonal anomalies are computed with respect to a mean annual cycle and filtered in the 20-90-day band. They are then regressed onto the precipitation averaged over the same domain, with varying lag. Radiative budgets produced on the basis of TRMM, Cloudsat, Calipso and CERES observations are used as a reference basis for comparison. Only CMIP5 coupled simulations from the EUCLIPSE models are considered hereafter.

Figure 8 shows the observed and simulated radiative fluxes at the top of the atmosphere (TOA) associated with an MJO in the eastern equatorial Indian Ocean. The observations exhibit near-cancellation between the longwave (LW) and shortwave (SW) signals almost in phase with the precipitation: additional albedo associated with the convective disturbance is compensated by the additional greenhouse effect of the clouds and moisture.

This behavior is reproduced by only the IPSL-B. The three other models simulate different patterns: a lagging and underestimated LW effect in the CNRM yields a maximum in TOA net (upward) flux that leads the precipitation maximum; a lagging LW effect and underestimated SW effect in the MPI-M yield a minimum TOA net flux that lags the precipitation maximum; an underestimated LW effect and a lagging SW effect yield a maximum of net TOA flux in the IPSL-A.

Figure 9 shows the TOA cloud radiative forcing (CRF), that is counted positively downward (positive fluxes heat the ocean-atmosphere system). The clear sky MJO signal is negligible in the SW, and it is a small heating term (CS fluxes are counted positively upward) in the LW that results from the moisture anomaly. This term is compensated by the net TOA CRF that results from compensating, large-scale SW (cloud albedo) and LW (cloud greenhouse) contributions that dominate the LW and SW all-sky fluxes. In the models, the CS fluxes are fairly well simulated, and the biases discussed on Figure 8. result from the cloud contributions. Despite a small precipitating signal compared to the observation, models such as IPSL-A simulate a realistic amplitude of the SW signal, indicating a bias in the cloud optical depth in the SW range. We can try to relate the radiative fluxes to the variables that are relevant for cloudiness and the atmosphere's optical depth. In most models, the total cloud amount and precipitable water covary, but in the CNRM the precipitable water anomaly is much smaller, and this contributes to the underestimation of LW CRF.

Figure 10 shows the surface radiative fluxes. The MJO is associated to a strong cooling of the surface due to the screening of incoming solar radiation by the convective disturbance. Indeed, the surface SW downward flux anomaly matches the TOA upward flux anomaly (see Fig 8) very closely: instead of reaching the surface, the solar incoming flux is reflected back to space. The model biases follow the biases observed at the TOA. The convective disturbance also causes additional greenhouse effect, with increased downward LW flux at the surface. This behavior is reproduced by the models, but its amplitude is overestimated.

Figure 11 shows the cloud and clear-sky contribution to the surface budget. The SW CRE is the dominating contribution, and the model biases follow the TOA biases. Both the CRF and CS fluxes contribute to the surface LW signal, with the latter larger than the former. Both are overestimated in the models, in particular in the CNRM model. In the other models, the surface LW CRF and CS fluxes tend to be in phase, while in the observation and CNRM the CS fluxes lead the convective maximum as a result of the moistening of the lower troposphere prior to the convection.

These results show that the model biases in radiative fluxes associated with the MJO are essentially due to the cloud radiative effects. They also show that there is no clear link between the ability of EUCLIPSE models to simulate the MJO and its ability to simulate the correct radiative LW and/or SW signal associated with the MJO. These results are the subject of an article in preparation.

2.2 Analysis of COOKIE experiments:

Theoretical and observational studies, as well as experiments with idealized models showed that moist-radiative feedbacks are crucial for convectively coupled equatorial waves (CCEWs) and especially the Madden-Julian-Oscillation (MJO). Crueger and Stevens (in preparation) investigate the role of cloud-radiative effects (CRE) in the MJO with three comprehensive atmosphere general circulation models (CNRM-CM5, MRI-CGCM3 and MPI-ESM). To switch

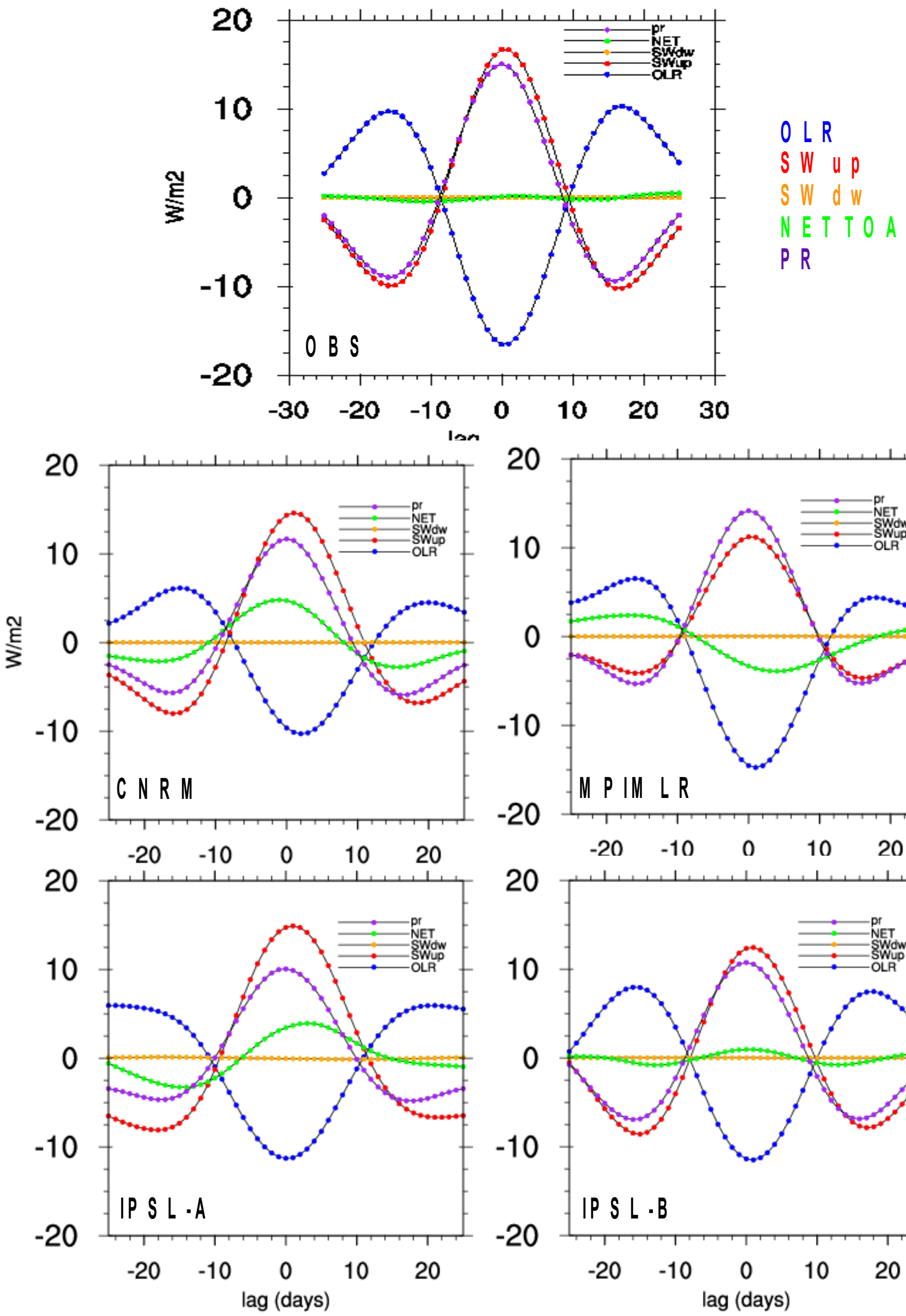

Figure 8: Top-of-the-atmosphere (TOA) radiative budget associated with the MJO in the observations (top panel) and four CMIP5 coupled models; "SW" stand for shortwave, "LW" for longwave, "up" indicates the upward flux and "dw" indicates the downward flux. The precipitation (PR) is represented as well for reference.

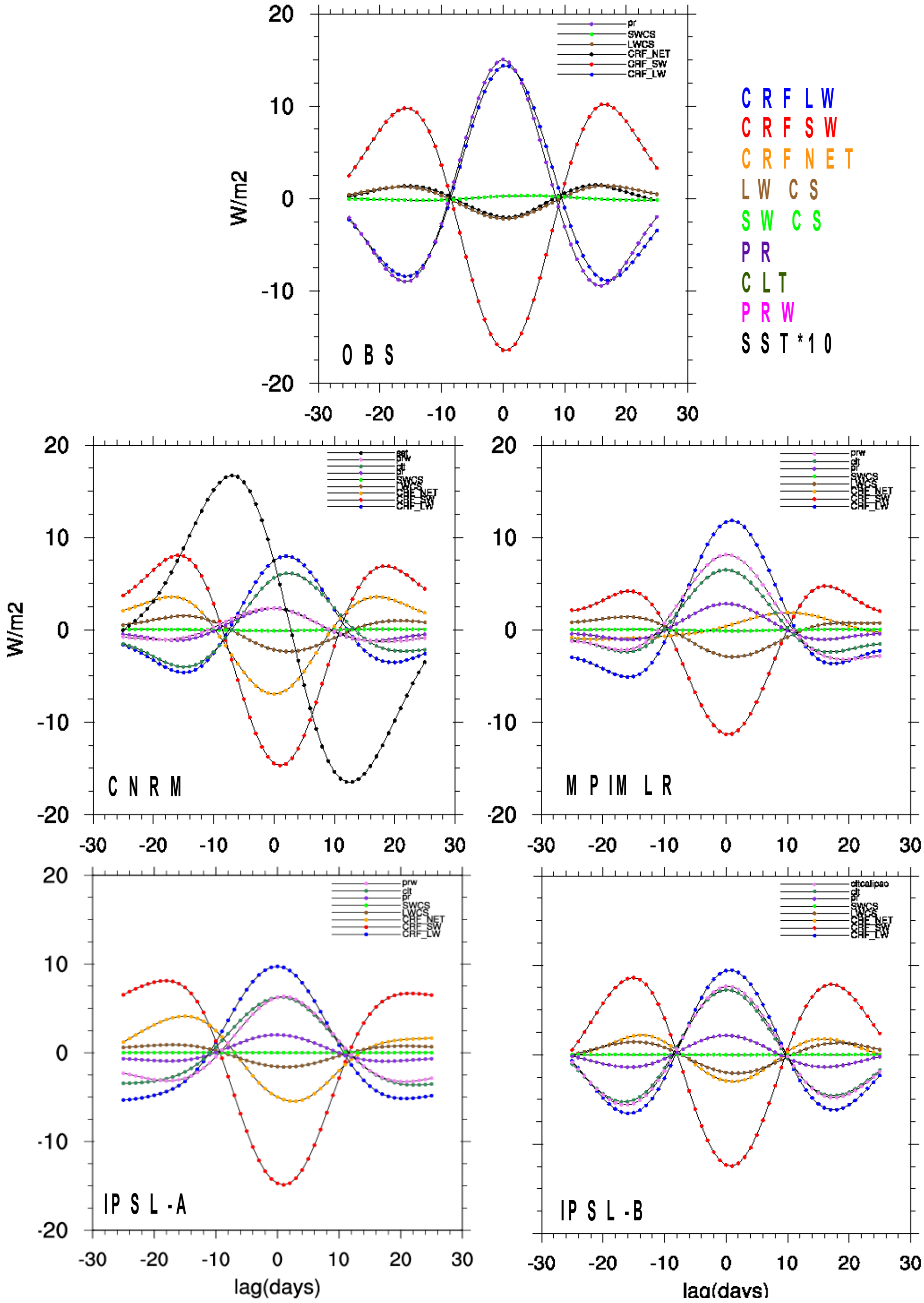

Figure 9: Top-of-the-atmosphere (TOA) cloud radiative forcing (CRF) and clear-sky (CS) fluxes associated with the MJO in the observations (top panel) and four CMIP5 models; "SW" stand for shortwave, "LW" for longwave, "up" indicates the upward flux and "dw" indicates the downward flux. The precipitation (PR), total cloud amount (CLT), precipitable water (PRW), and SST are represented as well for reference.

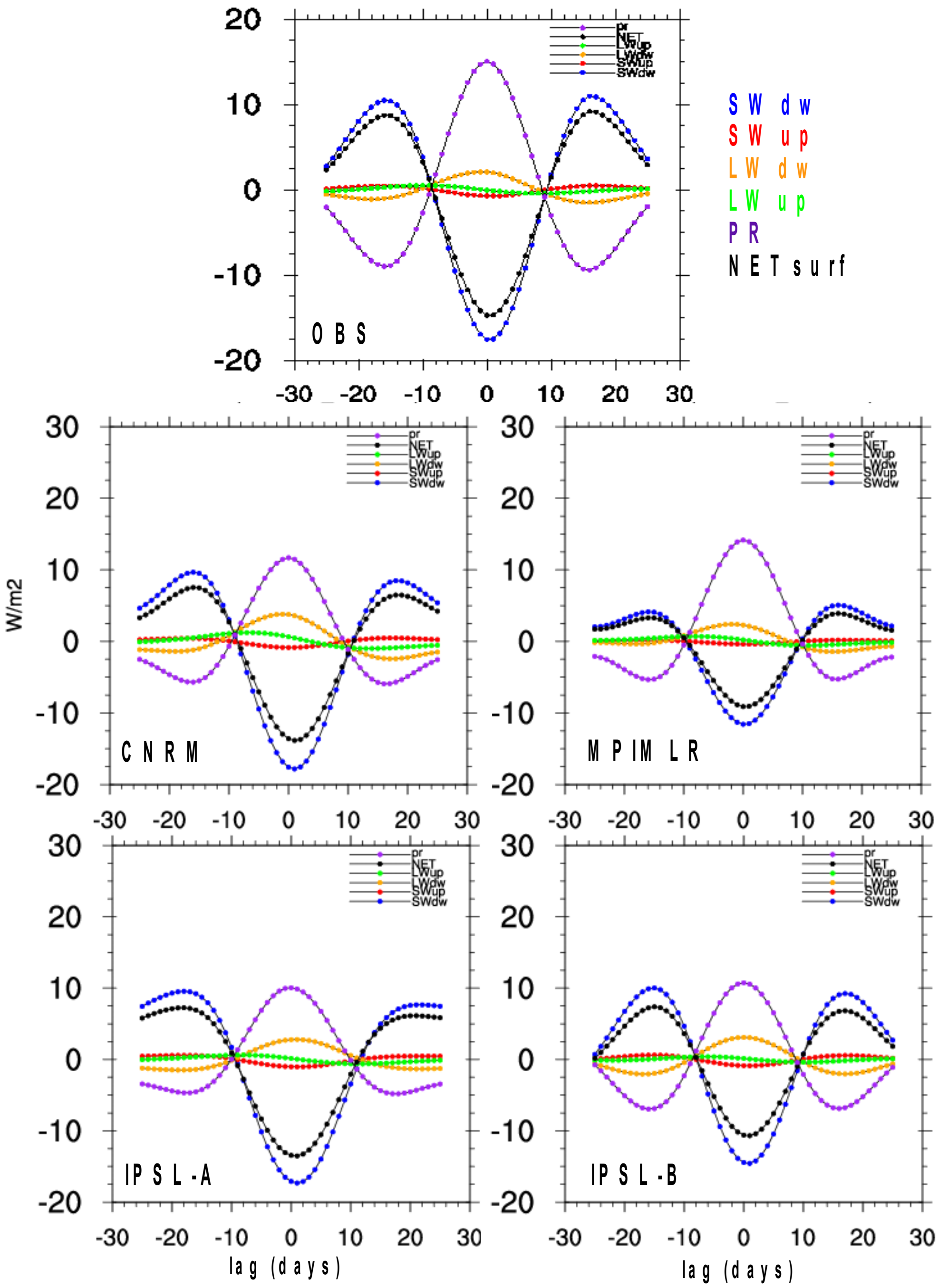

Figure 10: Surface radiative budget associated with the MJO in the observations (top panel) and four CMIP5 models; "SW" stand for shortwave, "LW" for longwave, "up" indicates the upward flux and "dw" indicates the downward flux. The precipitation (PR) is represented as well for reference.

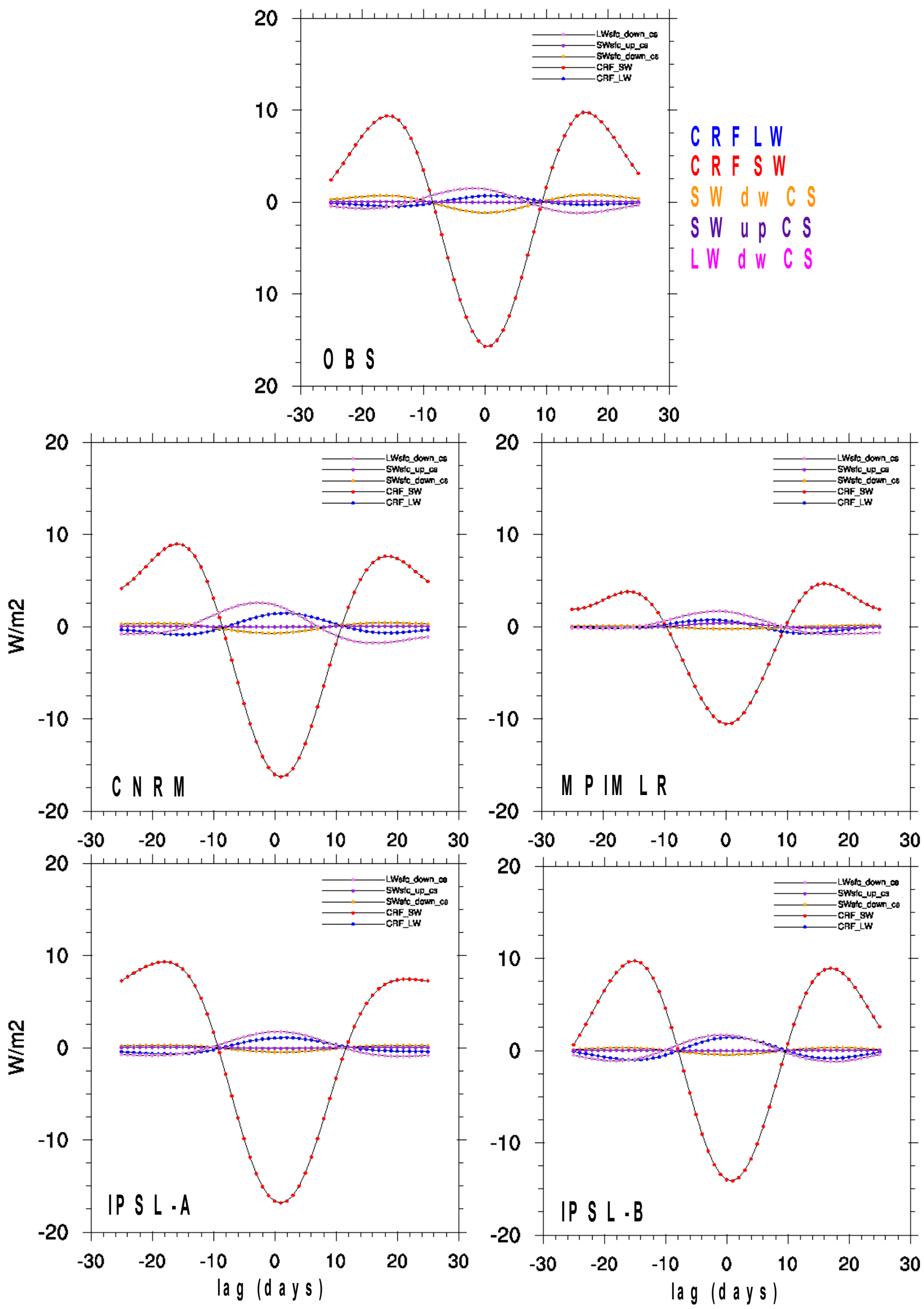

Figure 11: Surface cloud radiative forcing (CRF) and clear-sky (CS) fluxes associated with the MJO in the observations (top panel) and four CMIP5 models; "SW" stand for shortwave, "LW" for longwave, "up" indicates the upward flux and "dw" indicates the downward flux.

off cloud-radiative feedbacks, clouds are set to zero in the radiation code (so-called “clouds-off” or COOKIE experiments, Stevens et al. 2012). The analysis focuses on the mean state (precipitation and lower tropospheric winds) and on the heating profiles, which have both been previously found to be related to the MJO.

CRE strongly influence CCEWs. The models generally reveal more pronounced Kelvin waves in clouds-off compared to the control experiments including CRE (“clouds-on”). In contrast, the MJO weakens in clouds-off.

The mean state changes in response to switching-off CR-effects: Precipitation reveals a tendency to a double ITCZ (Intertropical Convergence Zone). The weakest tendency to a double ITCZ is found for MRI-CGCM3 that also shows the weakest decrease of MJO eastward propagation. The lower-tropospheric equatorial westerlies weaken in clouds-off for MPI-ESM and MRI-CGCM3, while for CNRM-CM5 the westerlies are shifted to the Indian Ocean. Overall, the link with the MJO is stronger for the ITCZ than for the zonal winds.

For MPI-ESM clouds-on, an amplification of the intraseasonal heating profiles were found compared to clouds-off. The total heating profile is dominated by convective heating. However, stratiform heating influences the shape of the profile, leading to a top-heaviness in clouds-on. The longwave heating profile tends to slightly decrease the maximum heating height. In contrast to clouds-on, clouds-off reveals a mid-heavy heating profile.

With respect to the MJO life cycle phases we found that the column-integrated radiative heating lags the vertically integrated moist static energy by 40 to 60 degrees. It suggests that the column-integrated cloud-radiative heating slows down the phase speed, and is therefore crucial for a realistic MJO phase speed. This is consistent with the analysis of CMIP5 models presented above.

References:

- Bony, S., and K. A. Emanuel, 2005: On the Role of Moist Processes in Tropical Intraseasonal Variability: Cloud–Radiation and Moisture–Convection Feedbacks, *Journal of the Atmospheric Sciences,* 62, 2770-2789.

- Crueger, T. and B. Stevens: Cloud-radiation effects on the Madden-Julian Oscillation. In preparation.

- Hung, M. P., J. L. Lin, W. Wang, D. Kim, T. Shinoda, and S. J. Weaver, 2013: MJO and Convectively Coupled Equatorial Waves Simulated by CMIP5 Climate Models, *Journal of Climate*, 26(17), 6185-6214.

- Raymond, D. J., 2001: A New Model of the Madden–Julian Oscillation, *Journal of the Atmospheric Sciences*, 58, 2807-2819.

3 Influence of the representation of clouds in models on the simulation of ENSO

3.1 ENSO in CMIP5 and CMIP3 models

The ability of CMIP3 and CMIP5 coupled ocean–atmosphere general circulation models (CGCMs) to simulate the tropical Pacific mean state and El Nino-Southern Oscillation (ENSO) have been analysed (Bellenger et al. 2014). The CMIP5 multi-model ensemble displays an encouraging 30 % reduction of the pervasive cold bias in the western Pacific (Fig 1.), but no quantum leap in ENSO performance compared to CMIP3. CMIP3 and CMIP5 can thus be considered as one large ensemble (CMIP3 + CMIP5) for multi-model ENSO and related tropical analysis.

The too large diversity in CMIP3 ENSO amplitude is however reduced by a factor of two in CMIP5 and the ENSO life cycle (location of surface temperature anomalies, seasonal phase locking) is modestly improved. Other fundamental ENSO characteristics such as central Pacific precipitation anomalies however remain poorly represented.

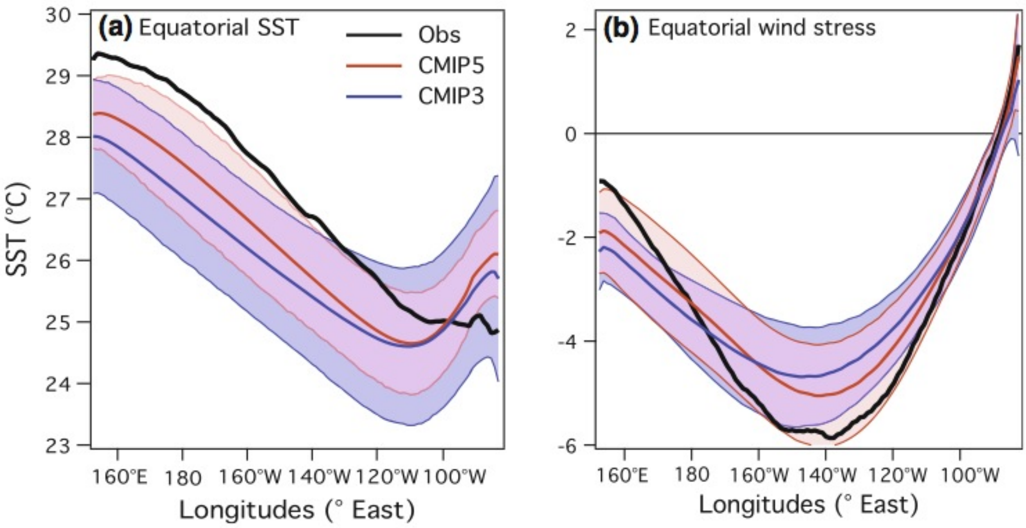

Figure 12: Average (a) SST (C) and (b) zonal surface wind stress (Nm^{-2}) at the equator (5S–5N) in the Pacific Ocean for ERA-40 (black) and CMIP3 (blue) and CMIP5 (red) ensemble mean. The inter model standard deviation is shaded in light colour.

The sea surface temperature (SST)-latent heat flux feedback is slightly improved in the CMIP5 ensemble but the wind-SST feedback is still underestimated by 20–50 % and the shortwave-SST feedbacks remain underestimated by a factor of two (Figure 13). The improvement in ENSO amplitudes might therefore result from error compensations.

The ability of CMIP models to simulate the cloud related SST-shortwave feedback, a major source of erroneous ENSO in CGCMs, is analysed and shows no major improvement from CMIP3 to CMIP5, in agreement with studies that show not major changes in cloud performance (e.g. Lauer and Hamilton 2013). In observations, this feedback is strongly nonlinear because the real atmosphere switches from subsident (positive feedback) to convective (negative feedback) regimes under the effect of seasonal and interannual variations. Only one-third of CMIP3 + CMIP5 models reproduce this regime shift, with the other models remaining locked in one of the two regimes (Fig.14).

The modelled shortwave feedback nonlinearity increases with ENSO amplitude and the amplitude of this feedback in the spring strongly relates with the models ability to simulate ENSO phase locking. These cloud related feedbacks are now routinely evaluated to understand ENSO properties in coupled GCMs.

3.2 Atmosphere response during ENSO and the role of clouds

Several studies point out the central role of the atmosphere general circulation model (GCM) response during ENSO in shaping the modelled ENSO (see for instance Guilyardi al. 2009 and Lloyd et al. 2011). Both dynamics (such as the Bjerknes feedback, Fig. 13a) and thermodynamics are involved in this response. Clouds are an integral part of the short wave feedback response (α_{SW}, Fig. 13c) as getting the correct shortwave response in the east Pacific requires not only to simulate the two broad dynamical regimes that occur in the region – the subsidence regime (Klein and Hartmann 1993), where low clouds prevail and α_{SW} is positive, and the convective regime (Ramanathan and Collins 1991; Bony et al. 1997), where convective clouds prevail and α_{SW} is negative, – but also their spatial repartition (Fig. 15a).

Motivated by findings that α_{SW} is the primary contributor to model thermodynamical damping errors, Lloyd et al. (2011, 2012) analysed this feedback in CMIP models. To understand the source of the α_{SW} errors, a new feedback decomposition method was introduced, breaking down the SW flux feedback into three individual, local responses:

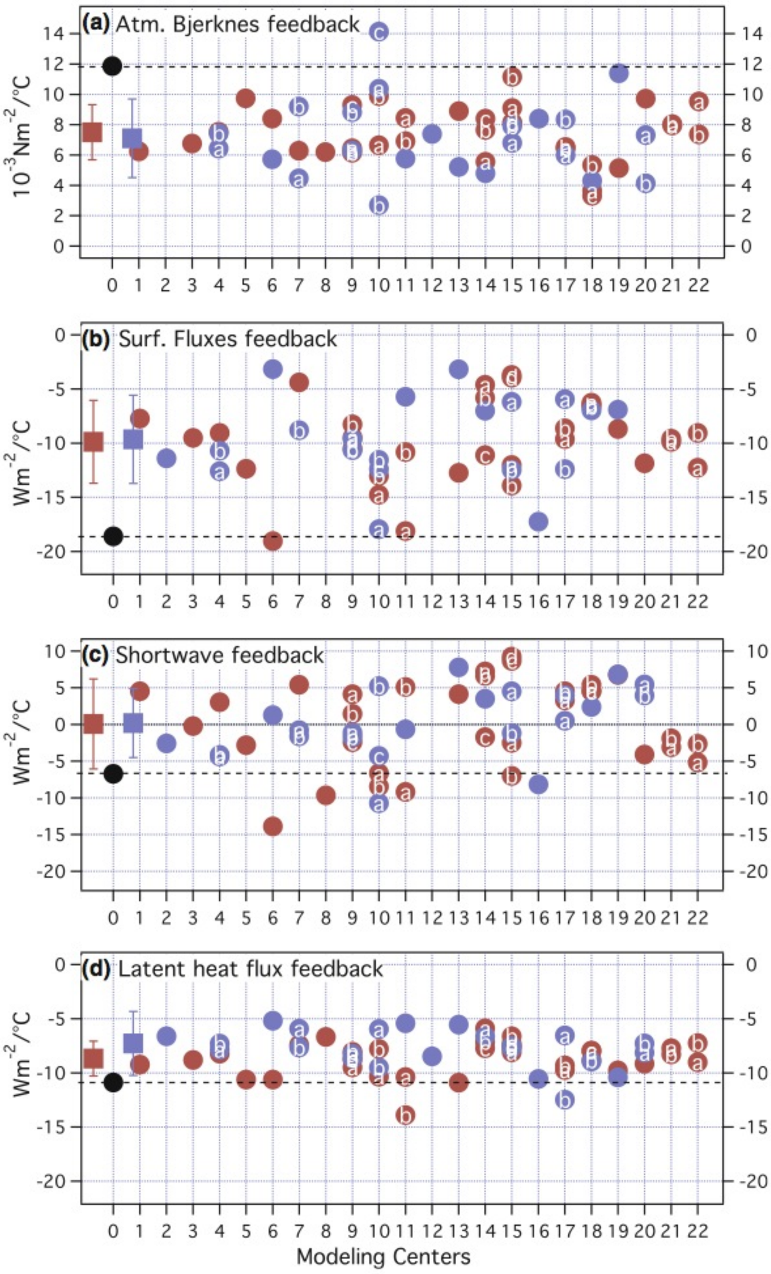

Figure 13: Atmosphere feedbacks during ENSO for pre-industrial control simulations–CMIP3 (blue) and CMIP5 (red). (a) atmospheric Bjerknes feedback, computed as the regression of Nino 4 wind stress over Nino3 SST (10^{-3} Nm^{-2}K^{-1}); (b) heat flux feedback, computed as the regression of total heat flux over SST in Nino3 (W m^{-2}K^{-1}); (c) Shortwave component of (b); (d) Latent heat flux component of (b). Reference datasets, shown as black solid circles and dashed lines, are ERA40 for (a) and OAFlux for (b), (c) and (d). See models and centres legend in Bellenger et al. (2014). The CMIP3 and CMIP5 multi-model mean are shown as squares on the left of each panel with the whiskers representing the inter-model standard deviation.

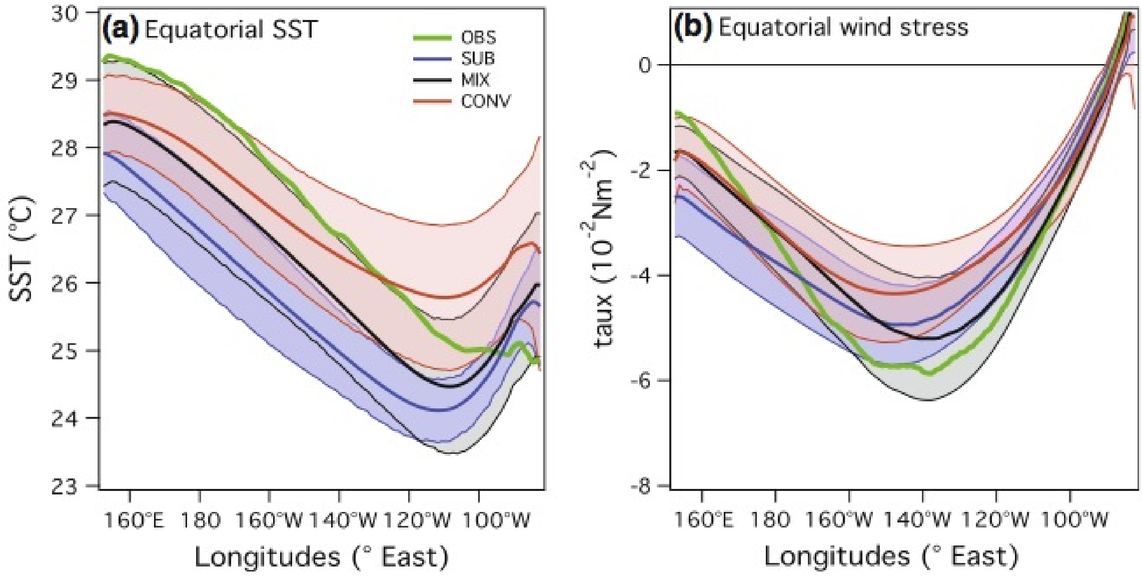

Figure 14: Average a SST (C) and b zonal surface wind stress (N m^{-2}) at the equator (5S– 5N) in the Pacific Ocean for ERA-40 (green) and subsidence (SUB) type models (blue), mixed convective-subsidence (MIX) type models (black) and convective (CONV) type models (red) ensemble mean. The inter model standard deviation for each model type is drawn in light colour.

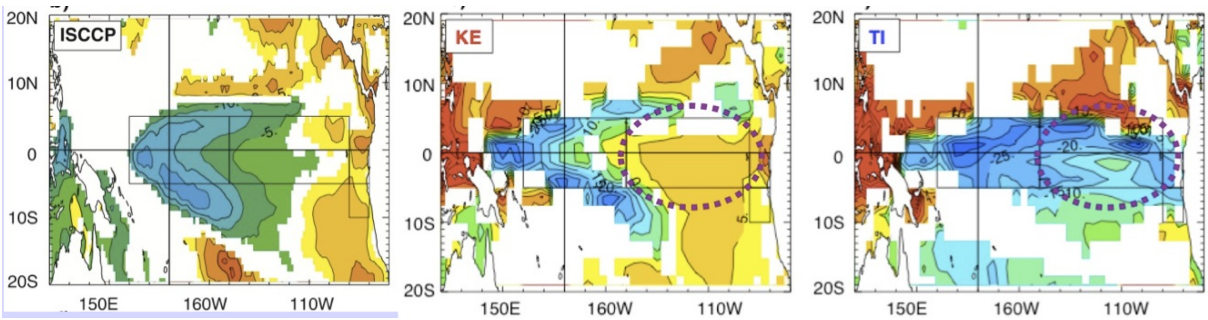

Figure 15: Spatial maps of the linear point wise SW flux regression against SST in the tropical Pacific Ocean (20N–20S, 110E–70W) in JASOND for ISCCP (left) and two models with opposite behaviours in the eastern Pacific: subsidence regime for the middle one and convective regime for the right one.

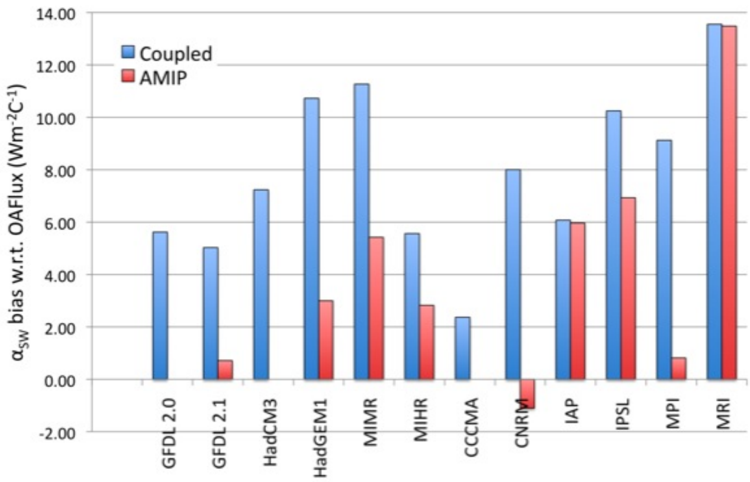

Figure 16: Fig. 5: α_{SW} biases (with respect to OAFlux) in the coupled (blue bars) and AMIP (red bars) CMIP3 simulations.

1) the dynamical response to SST dω_{500}/dSST, 2) the total cloud cover response to dynamics dTCC/dω_{500}, and 3) the SW flux response to clouds dSW/dTCC. It was shown that all coupled models underestimate the dynamical response during El Nios, a behaviour that is likely to contribute to the underestimated α_{SW} (Fig. **??**). Dynamical biases play a more important role in the coupled simulations than the AMIP simulations, in which cloud-related biases were found to be the main source of α_{SW} (Lloyd et al. 2011, Fig. **??**). This is because the large-scale circulation is no longer constrained by a prescribed SST forcing in the coupled simulations.

Changes in the dynamical response, dω_{500}/dSST, between the coupled and AMIP simulations exhibit a robust statistical relationship with the coupled–AMIP α_{SW} differences. Furthermore, it is shown that the coupled–AMIP differences in d$\omega_{500}/dSST$ can be directly related to the dynamical mean state coupled–AMIP changes. The coupled versus AMIP differences in the α_{SW} values are therefore linked to a shift in the dynamical mean state when the ocean and atmosphere models are coupled, a result which further underlines the important role of the dynamics in the coupled α_{SW} feedback.

Nevertheless, there are also large coupled model biases in the mean cloud properties over the equatorial Pacific, as supported by previous studies (Bony and Dufresne 2005; Sun et al. 2006, 2009) and found in the AMIP simulations (Lloyd et al. 2011). Biases in both the cloud response to dynamics, dTCC/dω_{500}, and the SW flux response to clouds, dSW/ dTCC, are likely to contribute to the SW flux response biases during model El Nios. An improvement in the coupled α_{SW} feedback will therefore only be possible with an improved simulation of both dynamical and cloud responses to SST variability in the eastern equatorial Pacific.

A large nonlinearity is found in the observed and modelled SW flux feedback, hidden when linearly calculating α_{SW}. In the observations, two physical mechanisms are proposed to explain this nonlinearity: 1) a weaker subsidence response to cold SST anomalies than the ascent response to warm SST anomalies and 2) a nonlinear high-level cloud cover response to SST. The shortwave flux feedback nonlinearity tends to be underestimated by the models, linked to an underestimated nonlinearity in the dynamical response to SST.

References :

- Bellenger H., E. Guilyardi, J. Leloup, M. Lengaigne, J. Vialard (2014). ENSO representation in climate models: from CMIP3 to CMIP5. *Clim. Dyn.*, **42**, 1999-2018.

- Guilyardi E., P. Braconnot, F.-F. Jin, S. T. Kim, M. Kolasinski, T. Li and I. Musat (2009). Atmosphere feedbacks during ENSO in a coupled GCM with a modified atmospheric convection scheme. *J. Clim.*, **22**, 5698-5718.
- Lloyd, J., E. Guilyardi and H. Weller (2011), The role of atmosphere feedbacks during ENSO in the CMIP3 models, Part II: using AMIP runs to understand the heat flux feedback mechanisms, *Clim. Dyn.*, **37**, 1271-1292.
- Lloyd J., E. Guilyardi, H. Weller, (2012). The Role of Atmosphere Feedbacks during ENSO in the CMIP3 Models. Part III: The Shortwave Flux Feedback. *J. Clim.*, **25**, 4275-4293.

Other references:

Bony, S., and J.-L. Dufresne, 2005: Marine boundary layer clouds at the heart of tropical cloud feedback uncertainties in climate models. Geophys. Res. Lett., 32, L20806.

Bony, S. K.-M. Lau, and Y. C. Sud, 1997: Sea surface temperature and large-scale circulation influences on tropical greenhouse effect and cloud radiative forcing. J. Climate, 10, 2055–2077.

Klein, S. A., and D. L. Hartmann, 1993: The seasonal cycle of low stratiform clouds. J. Climate, 6, 1587–1606.

Ramanathan, V., and W. Collins, 1991: Thermodynamic regulation of ocean warming by cirrus clouds deduced from observations of the 1987 El Nino. Nature, 351, 27–32.

Sun, D.-Z., and Coauthors, 2006: Radiative and dynamical feed- backs over the equatorial cold tongue: Results from nine atmospheric GCMs. J. Climate, 19, 4059–4074.

Sun, D.-Z., Y. Yu, and T. Zhang, 2009: Tropical water vapour and cloud feedbacks in climate models: A further assessment using coupled simulations. J. Climate, 22, 1287–1304.

4 Influence of large-scale circulation, cloud and land surface processes on European (and North American) temperatures

Objectives

The purpose of this deliverable is to document the performance of the CMIP5 climate models in simulating present-day European temperatures (based on historical simulations driven by both natural and anthropogenic radiative forcings), to investigate their projected changes (under several 21st century Radiative Concentration Pathways but with a particular emphasis on the most severe RCP8.5 scenario), and to understand the associated model uncertainties (i.e. the intermodel spread). Beyond seasonal mean temperature, a particular attention is paid to intraseasonal variability and extremes (i.e. cold spells and heat waves) which may induce greater socio-economic and environmental impacts than changes in mean climate. Ultimately, we look for robust statistical relationships between the behaviour of climate models in present-day versus future climates in order to identify potential or effective (i.e. using available observations) emerging constraints on climate projections. Although Europe (especially Central Europe) is fairly representative of many summer mid-latitude areas, it is strongly affected by anthropogenic aerosols so that the North American temperatures are also analysed. A detailed physical understanding of both model biases and uncertainties is crucial, not only to guide further model developments but also to avoid the use of spurious observational constraints. For this purpose, an original methodology based on a weather regime approach has been developed to distinguish between biases or changes due to large-scale atmospheric dynamics and those due to local processes. In this report, the focus is mainly on cloud and land surface processes, whose local radiative and heat effects on the surface energy budget represent major contributions to the inter-model spread.

Data and methods:

We use outputs from more than 30 CMIP5 models, but depending on data availability, not all models are included in all analyses. We focus on both the winter (DJFM) and summer (JJAS) seasons. Models are evaluated by comparing their historical simulations (HIST) with observations over the 1979-2008 period. This period was chosen to also make use of the idealized AMIP-type experiments driven by prescribed observed SST and thereby assess the contribution of the ocean-atmosphere coupling to the atmospheric and land surface biases. Climate change is assessed from differences between HIST and the 2070-2099 period in 21st century projections, for which we mostly use the RCP8.5 concentration scenario (but also the less severe RCP2.6 and RCP4.5 scenarios for some specific analyses). Historical runs ending in 2005 were completed by corresponding RCP8.5 runs over the period 2006-2008. For practical reasons, we only consider one run per model and per experiment (r1i1p1 in CMIP5 standards). A set a coordinated atmosphere-only CFMIP experiments, in which the cloud radiative effects are switched off, is also used to further document the cloud contribution to errors (uncertainties) in present-day (future) temperatures. Besides mean surface air temperature (*tas*) and its daily minimum (*tasmin*) and maximum (*tasmax*) values, we analyse the diurnal temperature range (*DTR=tasmax-tasmin*) and the inter-diurnal temperature variability ($ITV=|tas_{d+1}-tas_d|$). The North Atlantic weather regimes are defined from a cluster analysis of the daily maps of mid-troposphere geopotential height (*Z500*). The breakdown of model biases and responses into large-scale and local components is described in Cattiaux et al. (2013a). As far as monthly data is concerned, all-sky and clear-sky surface radiative fluxes are used to compute the cloud radiative effect (CRE or CRF) and the surface albedo while turbulent fluxes are used to define the evaporation fraction (*EF=H/(H+LE)*). Multi-model ensemble (MME) statistics are computed after interpolating all model outputs onto a common intermediate (1.4) horizontal grid using a conservative scheme. To get rid of model biases, cold spells and heat waves are defined using a quantile exceedance approach and described using common statistics: intensity, duration, extent as well as their product to characterize the overall severity of the regional events.

Main results:

(a) Present-day climate (1979-2008)

Starting with model biases in seasonal mean surface air temperature, Fig. 17 shows that the CMIP5 MME underestimates the winter temperature over northern Europe but with a large inter-model spread, as also revealed by the individual model biases averaged over the whole European domain. In contrast, models tend to overestimate the summer temperature, especially over central and eastern Europe. The inter-model spread is again substantial although slightly weaker than in winter. Fig. 17c and f also show that most CMIP5 models tend to underestimate the DTR in both winter and summer, although some models (especially INM in summer) can overestimate it.

Biases in the pattern and/or frequency of the North Atlantic weather regimes are not strong enough and/or not enough model-dependent (for instance most models show an underestimated frequency of blockings in both seasons) to contribute substantially to the inter-model spread in present-day European temperatures (*Cattiaux et al. 2013b*). Temperature biases are dominated by non-dynamical local processes that are not specific to the European sector. They are even more pronounced in AMIP-type simulations (Fig.18abc) since they are often mitigated by a cold bias over the mid-latitude northern oceans in the CMIP5 simulations.

The inland warm bias is associated with a strong underestimation of the amplitude of the negative shortwave cloud radiative effect at the land surface (Fig.18def), especially over Central Europe and the US Great Plains. Further analyses over North America (*Douville et al. 2014*) also emphasize a clear relationship with summer precipitation

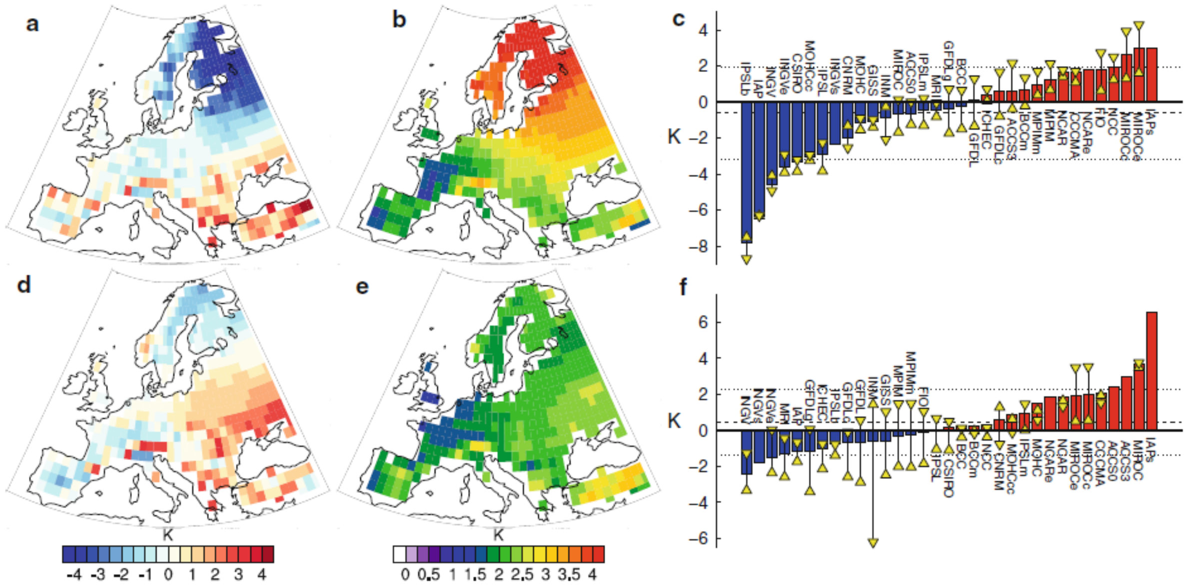

Figure 17: (a) Ensemble-mean temperature bias in winter, relative to EOBS. (b) Inter-model standard deviation (σ). (c) Individual model biases averaged over continental Europe (i.e. grid points in a and b), and sorted by increasing order. Ensemble mean (dashed line) and $\pm 1\sigma$ departures (dotted lines) are added. Upward (downward) triangles indicate corresponding values for daily maximum (minimum) temperatures, when available. (d–f) Same as (a–c) for summer (from *Cattiaux et al. 2013b*).

(not shown), whose deficit can translate into a warm bias through an underestimated evaporative fraction (Fig 3a). Additional AMIP-type simulations in which the cloud radiative forcing has been switched off have been also conducted by the EUCLIPSE participants in the framework of the CFMIP2 intercomparison project. Although highly idealized, these experiments confirm the major influence of cloud radiative effects on the summer temperature biases (Fig.19b).

(b) Future climate

Moving to the mean temperature change simulated in the RCP8.5 scenario, Fig.20 shows a maximum winter warming over northern Europe, but with a large inter-model standard deviation. In summer, the strongest MME anomalies are simulated over southern Europe (where they are much larger than in winter) with a maximum spread north of the area with maximum warming. Individual model results also emphasize a general decrease in DTR in winter and, on the contrary, a general increase in summer, thereby revealing different dominant physical processes behind the daily mean surface warming.

Although generally significant, changes in the pattern and/or frequency of the North Atlantic weather regimes are too weak and/or too similar to be a major contributor to the inter-model spread in projected European temperatures (*Cattiaux et al. 2013b*). Most models show a decreased (increased) frequency of the blocking and Atlantic Ridge regimes in winter (summer). There is also a relative consensus about the response of the negative NAO regime in winter (increased frequency) and summer (decreased frequency), while the response of the positive NAO regime in winter is more model-dependent, in contrast with the CMIP3 results and highlighting the non linearity of the North Atlantic variability. Note that the role of large-scale dynamics would have been probably more obvious if the breakdown methodology had been applied after normalizing the grid-cell temperature anomalies by the projected global warming.

Beyond changes in the large-scale circulation, the simulated seasonal temperature response is highly dependent

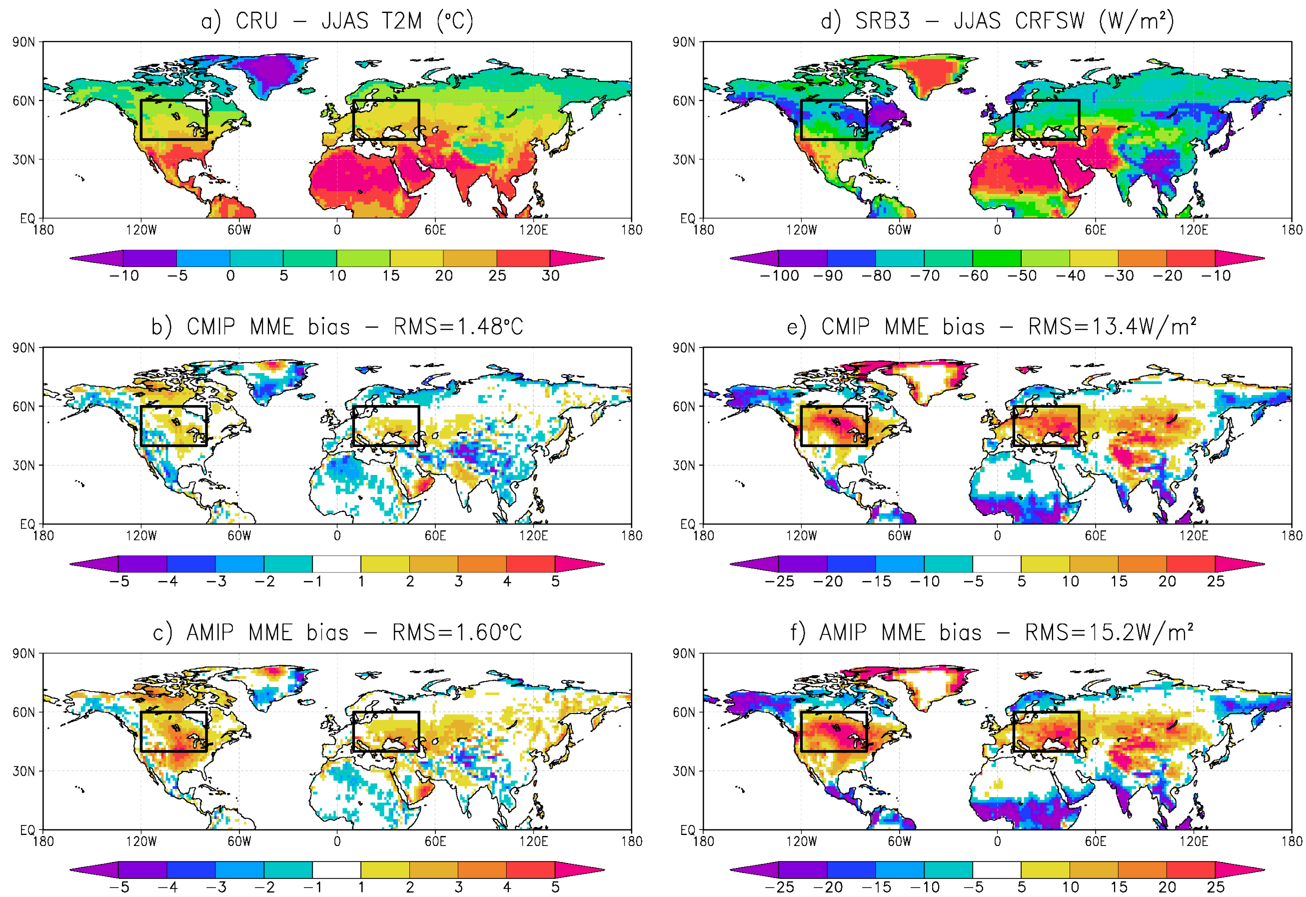

Figure 18: (a) Observed climatological summer near surface temperature, (b) MME mean biases in CMIP5 models, (c) MME mean biases in corresponding AMIP-type simulations, (d,e,f) same for the surface shortwave cloud radiative effect. Observations are from the CRU TS3.1 climatology for temperature and from the SRB satellite data for the shortwave CRF. Black rectangles denote the US Great Plains and Central Europe domains where the MME CRF biases show maximum positive values (from *Douville et al. 2014*).

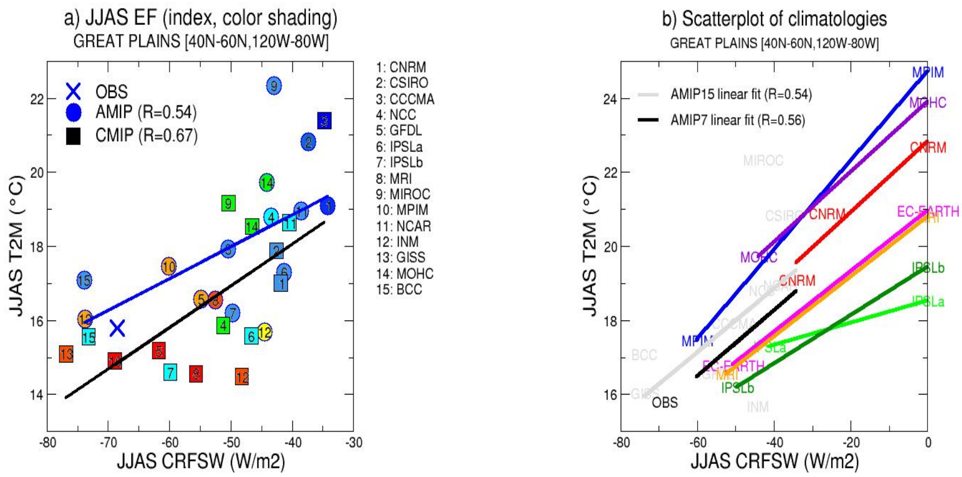

Figure 19: The higher the underestimation of the shortwave cloud radiative effect amplitude, the warmer the bias (not excluding an important role of land surface processes). Scatterplots of 1979-2008 JJAS climatologies from CMIP5 models averaged over the US Great Plains: (a) T2M vs CRFSW in observations (cross), 15 AMIP simulations (circles, linear fit in blue), and 15 historical simulations (squares, linear fit in black). Colors in symbols denote the corresponding EF (Evaporative Fraction) climatology averaged over the same domain with blue (red) colors showing weak (strong) EF values for present-day climate; (b) T2M vs CRFSW in observations, 15 AMIP simulations (linear fit in grey) including 7 models (other color models, linear fit in black) that have also been run without cloud radiative forcing (Off AMIP simulations shown along the right y-axis), individual model linear fit are also shown using the AMIP and Off AMIP simulations, as well as another idealized simulation in which only the low-level cloud radiative forcing has been switched off for the CNRM model (from *Douville et al. 2014*).

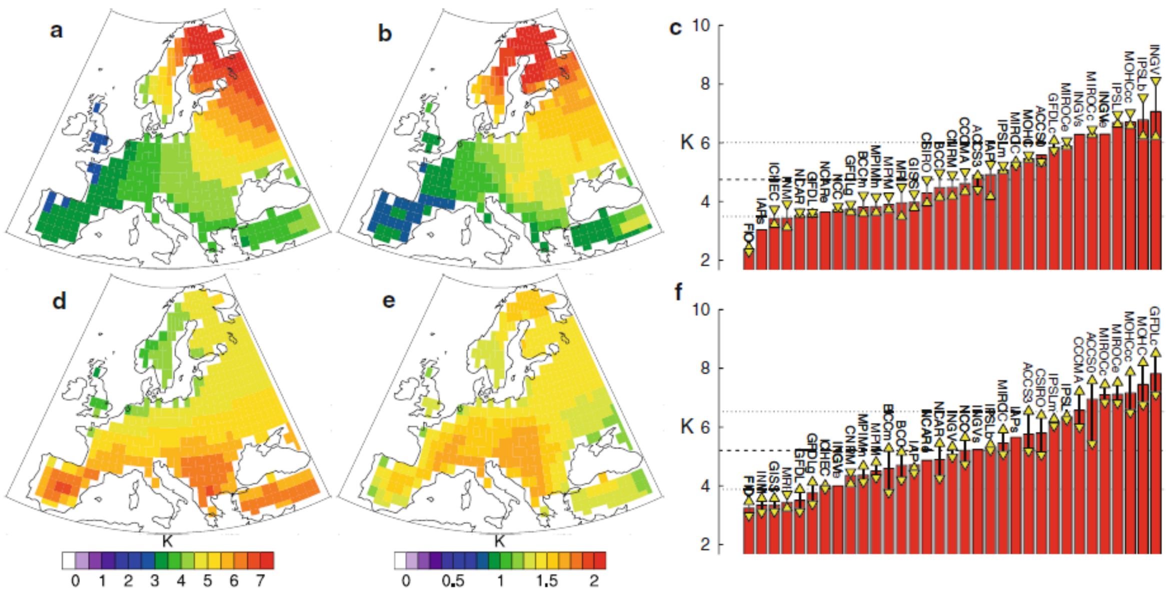

Figure 20: a Ensemble-mean temperature change in winter, between RCP85 and HIST. b Inter-model standard deviation (σ). c Individual model changes averaged over continental Europe (i.e. grid points in a and b), and sorted by increasing order. Ensemble mean (dashed line) and ± 1σ departures (dotted lines) are added. d–f Same as a–c for summer (*from Cattiaux et al. 2013b*).

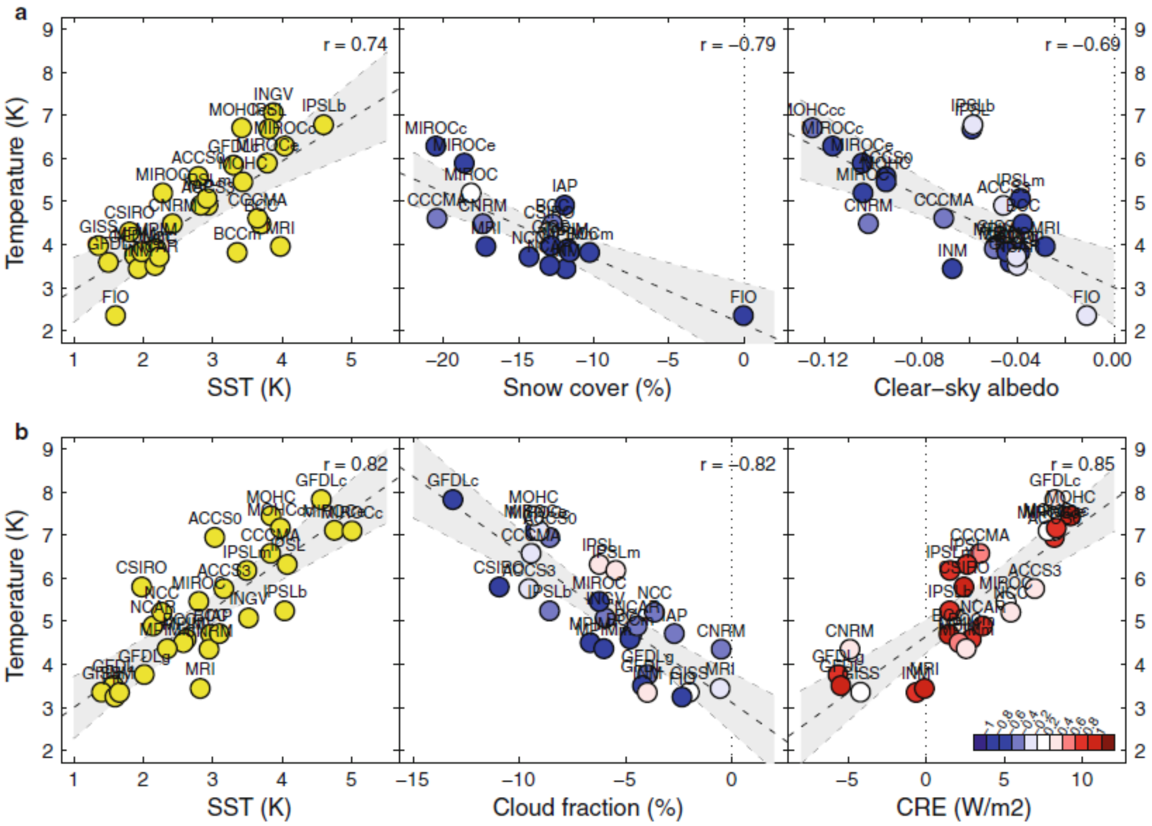

Figure 21: a European averages of winter temperature changes (RCP85-HIST) plotted versus projected responses in (1) North-Atlantic SST, (2) snow cover, and (3) clear-sky surface albedo. b European averages of summer temperature changes (RCP85-HIST) plotted versus projected responses in (1) North-Atlantic SST, (2) cloud fraction, and (3) surface cloud radiative effect (CRE). Fill colors of points indicate the spatial correlation over the European domain (see scale in b, rightmost panel). Dashed regression lines are plotted when a 10 %-significant correlation is found, together with the 95 % confidence interval in grey shading (from *Cattiaux et al. 2013b*).

on the North Atlantic surface warming (through the advection of oceanic air masses by the dominant westerlies), but also on local processes such as the snow albedo feedback in winter or the cloud radiative feedback in summer (Fig.21). Such regional feedbacks are potentially sensitive to model biases. For instance, the models that simulate the most extensive snow cover over Europe in winter can exhibit the strongest positive albedo feedback (at least in the most severe RCP8.5 scenario), which contributes to the anti-correlation between the present-day temperature and the projected warming (not shown). Similarly, the models that simulate a strong cloud cover in summer are likely to project a stronger reduction of the negative cloud radiative effect, which might contribute to the positive correlation between the present-day temperature and the projected warming (cf. section c).

Beyond Europe, the projected changes in summer mean temperature over the US Great Plains also show a significant relationship with changes in the surface cloud radiative effect, especially the shortwave component (*Douville et al. 2014*). Yet, this link is less pronounced than in the subtropical maritime anticyclones such over the northeast subtropical Pacific, and even than at the global scale (Fig.22). Moreover, a similar relationship is found with changes in the evaporative fraction and the role of the land-atmosphere coupling in the regional cloud response remains an open question.

Beyond seasonal mean temperature, the daily temperature distribution also shows substantial changes that cannot be fully accounted for by a simple shift of the whole distribution (e.g. *Schoetter et al. 2014*). In winter, the

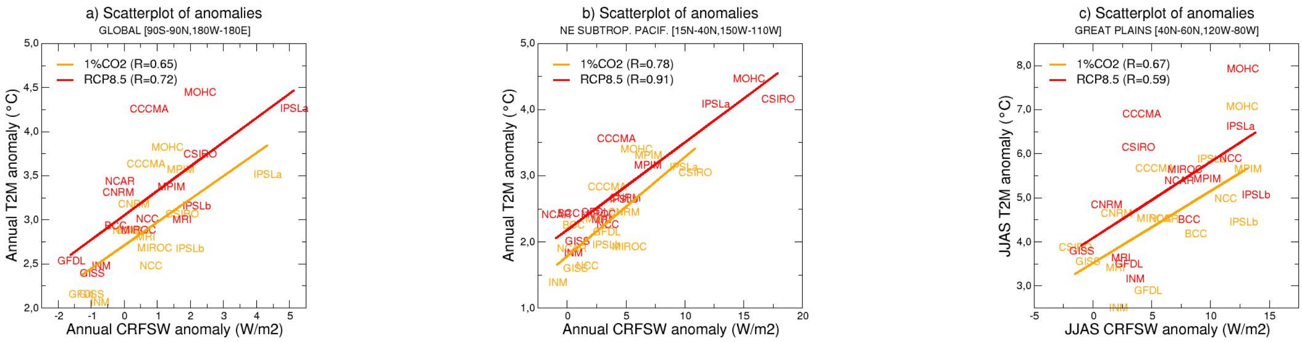

Figure 22: Projected near surface temperature changes (RCP85-HIST in red, years 111-140 minus years 11-40 of +1%CO2 experiments in orange) versus projected response in surface shortwave cloud radiative effect: (a) global annual mean anomalies, (b) annual mean anomalies over the northeast subtropical Pacific, (c) summer (JJAS) mean anomalies over the US Great Plains.

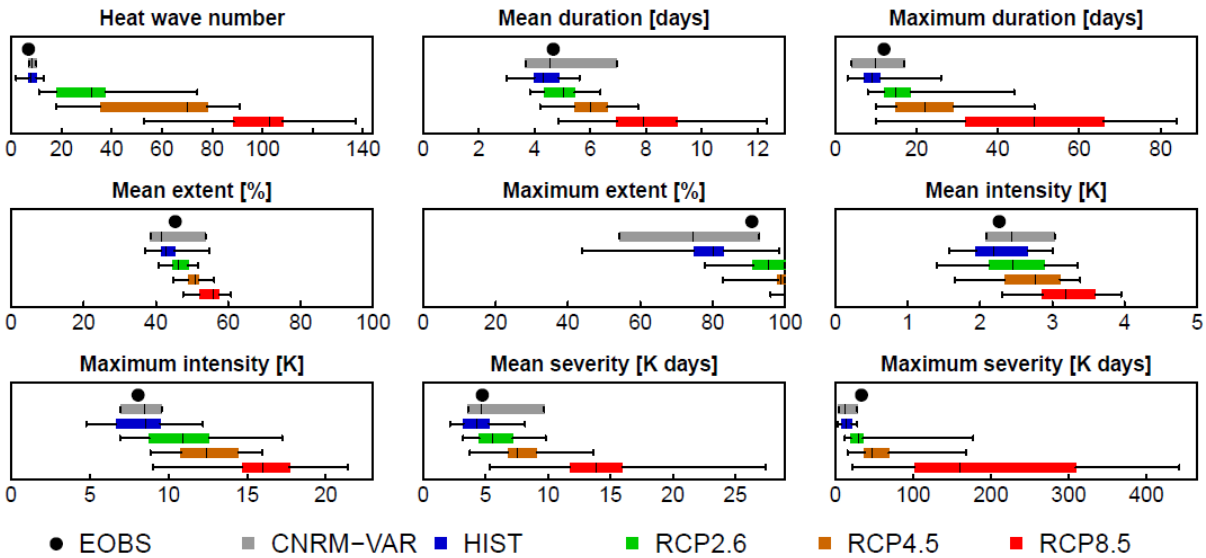

Figure 23: Boxplot of mean heat wave characteristics simulated by CMIP5 models for present-day climate (HIST) and three RCP scenarios. The grey bar indicates the range of present-day characteristics due to the internal variability simulated by the CNRM-CM5 model. Severity is defined as the product of duration, extent and intensity. Heat waves are defined relative to local temperature thresholds and minimum extent and duration, see *Schoetter et al., 2014,* for details.

western Europe cold spells (WECS) show a substantial decrease in frequency, duration and intensity when defined using the present-day 10th percentile of the daily minimum temperature distribution for both present-day and future climates. The intensity response is however model-dependent, strongly anti-correlated with the projected seasonal mean warming, and therefore influenced by both cloud and snow feedbacks (*Peings et al. 2012*). More recently, the western Europe heat waves in summer have been also explored using a larger number of CMIP5 models and more RCP scenarios (*Schoetter et al. 2014*). Not surprisingly, the results indicate an increase in heat wave duration, extent and intensity that is again model-dependent and particularly large for the most severe RCP8.5 scenario (Fig.22).

Besides cold spells and heat waves, other indicators of the high-frequency temperature variability have been analysed such as the diurnal temperature range (DTR) and the day-to-day temperature variability (ITV). Both indicators mostly show an increase in summer. The magnitude is again model-dependent and shows a significant statistical link with the response of the evaporative fraction (and therefore precipitation), as well as with the response of total cloud cover for the DTR (Fig.24, *Cattiaux et al. 2014*). Constraining the cloud and land surface responses is therefore

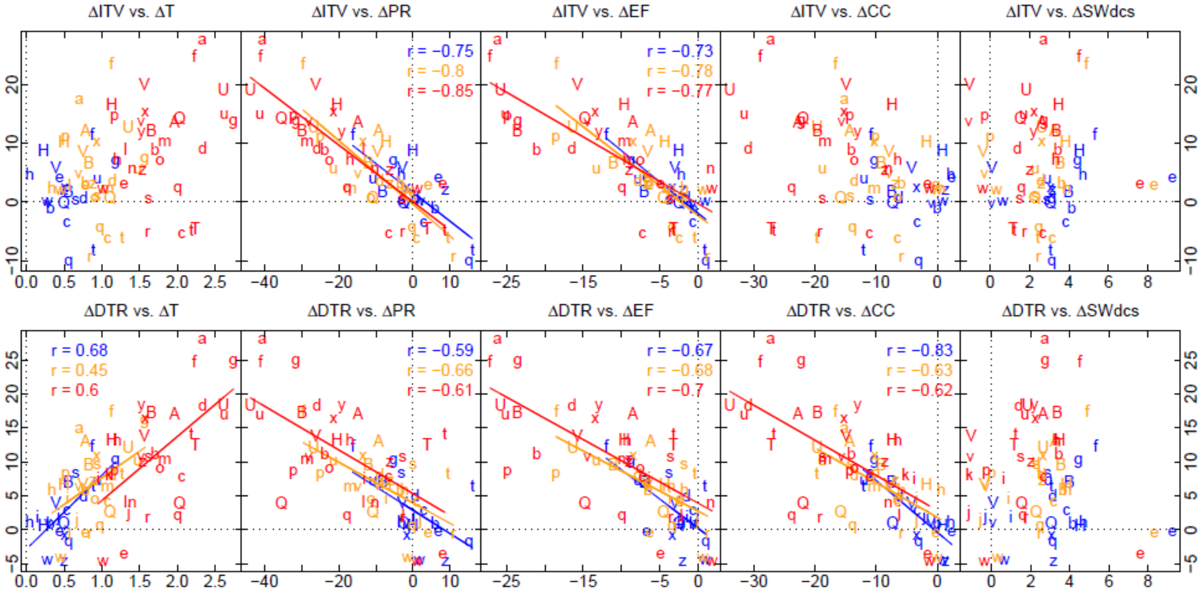

Figure 24: Projected relative changes in day-to-day temperature variability (ITV, top) and diurnal temperature range (DTR, bottom) as a function of projected relative changes in temperature (T), precipitation (PR), evaporative fraction (EF), cloud cover (CC) or clear-sky downward solar radiation (SWdcs). Each symbol represents one model in one scenario (R2.6 in blue, R4.5 in orange, R8.5 in red). For each scenario, regression lines are added when 95%-significant. For both x and y axes, changes are expressed in % wrt HIST values (from *Cattiaux et al. 2014*).

a priority for narrowing uncertainties, not only in seasonal mean temperature projections but also in DTR and ITV projections.

(c) Emergent constraints

Different metrics can be used to constrain global to regional climate projections through the identification of emergent statistical relationships between the behaviour of climate models in recent and future climates. Beyond annual or seasonal mean model biases, metrics about the annual cycle, the interannual variability or the multi-decadal trends are obvious potential candidates. But the lack of reliable, homogeneous, and long enough instrumental records is a major difficulty. Moreover, the strong internal variability of regional climate is another obstacle for deriving emergent constraints from recent trends in observed timeseries (e.g. *Cattiaux et al. 2014*).

Coming back to the study by Cattiaux et al. (2013b), the winter and summer responses of European temperatures show contrasted sensitivity to model biases (Fig.25) with cold models showing the strongest warming in winter while a reverse statistical relationship is found in summer. Model biases are therefore useful to understand and constrain the projected temperature anomalies, but the statistical relationships are not strong enough to obtain a major reduction in model uncertainties so that other metrics should be investigated.

Fig.25 also shows a strong linear relationship between the projected warming at the European versus global scale, especially in summer. Constraining the global climate sensitivity is therefore an efficient way to constrain projected regional temperature changes. Reasons for the weaker relationship in winter have not been investigated in details but include a stronger contribution of the large-scale dynamics to the inter-model spread (*Cattiaux et al. 2013b*) and a stronger internal variability over Europe (hence the need of several simulations for a robust estimate of regional warming in winter). Conversely, it could also suggest that the processes at work over Europe in summer (including cloud but also soil moisture feedbacks) are particularly relevant for understanding the global climate sensitivity of the

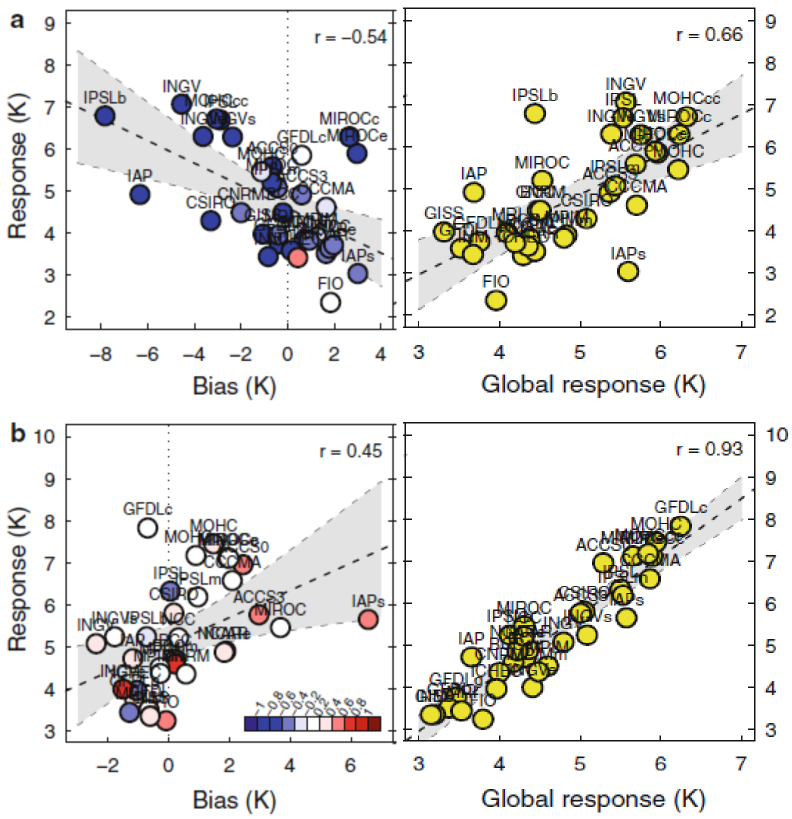

Figure 25: (a) European averages of winter temperature changes (RCP85-HIST) plotted versus present-day biases (HIST-EOBS, left panels) or projected global warming during the same season (right panels). (b) Same as a for summer. Fill colors of points indicate the spatial correlation over the European domain (see color scale in b). Dashed regression lines are plotted when a 10 %-significant correlation is found, together with the 95 % confidence interval in grey shading (*from Cattiaux et al. 2013b*).

CMIP5 models.

Moving to the US Great Plains, Fig.26 also looks for potential relationships between the present-day model climatologies and the projected near surface temperature anomalies in the RCP8.5 concentration scenario. The scatterplots indicate that, beyond temperature biases themselves, other model biases (including in CRFSW but also in the evaporative fraction or in precipitation) can be used to constrain the projections. Precipitation biases here appear as the most effective constraint and explains about half of the inter-model spread in the regional temperature projections. Note that the biases shown in Fig.26 are not independent and cannot be considered as additive constraints but that the results suggest the need for multi-variate (and process-oriented) constraints of climate change.

Prospects:

It has long been recognized that differences in simulated cloud feedbacks are a primary source of uncertainties for the model-predicted near-surface temperature change induced by increasing concentrations of greenhouse gases such as CO_2. While cloud processes indeed represent the main source of uncertainty in the projected global warming, they do not necessarily play such a dominant role at the regional scale and/or when analysing changes in temperature variability rather than in mean climate. The inter-model spread in climate sensitivity is dominated by the tropical cloud feedback but shows a weaker contribution of the mid-latitude clouds (e.g. Vial et al. 2014). Land surface processes also play a key role in the projected changes of summer mid-latitude temperatures (e.g. Seneviratne et al. 2013), but they are not fully accounted for in the breakdown of climate sensitivity uncertainties given the focus on

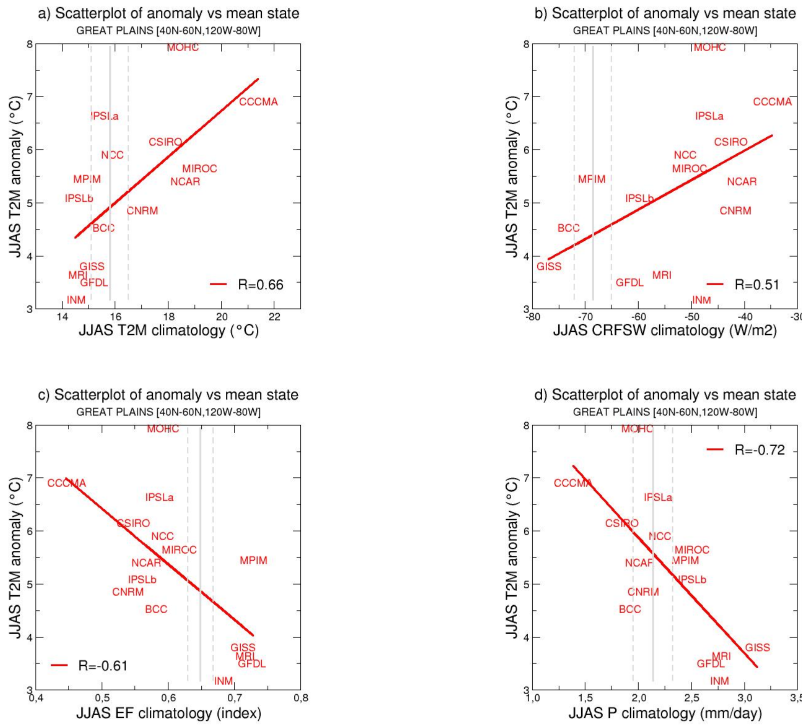

Figure 26: Scatterplots of RCP8.5 JJAS near surface temperature anomalies (C) projected over the US Great Plains in a subset of 15 CMIP5 models versus 1979-2008 JJAS climatologies of (a) near surface temperature (C), (b) surface shortwave cloud radiative effect (W/m²), (c) evaporative fraction (EF=LE/(H+LE)), and (d) precipitation (mm/day) averaged over the same domain and over the 1979-2008 period. Grey vertical lines indicate an observed estimate of the climatology (thick solid) +/-1 standard deviation of interannual variability (thin dashed). Observations are here derived from CRU, SRB, ERA-Interim and GPCC in a,b,c,d respectively.

radiative processes. Eventually, inter-model discrepancies in the response of the large-scale atmospheric dynamics also contribute to uncertainties in regional warming, albeit to a minor extent.

In theory, constraining the cloud feedbacks and, thereby, the global climate sensitivity is probably the most efficient way to constrain regional changes in both mean and extreme temperatures. This is however a long-standing issue and, in practice, parallel initiatives are required to narrow more efficiently and rapidly the inter-model spread in the temperature projections. Disregarding the observation requirements, three types of metrics can be used for this purpose, which are related to mean climate (e.g. Stegehuis et al. 2013), interannual variability (Bo and Terray 2014) and trends (e.g. Cattiaux et al. 2014) respectively. However, in practice, the instrumental record is often too short and/or the signal-to-noise ratio too low to make use of the observed trends, at least without implementing a clean detection-attribution statistical methodology. Moreover, some land surface variables such as soil moisture and the evaporative fraction are poorly constrained by satellite observations and land surface reanalyses so that even the use of model biases and/or interannual variability is not straightforward.

Beyond statistical relationships between the model behaviours in present-day versus future climates, coordinated simulations are necessary for a better understanding of model biases and/or uncertainties in climate projections. Besides the COOKIE experiments performed within the EUCLIPSE project (e.g. Douville et al. 2014) and the GLACE-CMIP5 experiments performed within the EMBRACE project (Seneviratne et al. 2013), other sensitivity tests could be organized in the model intercomparison projects that will flourish around the forthcoming CMIP6 DECK experiments (Meehl et al. 2014). Like the mitigation of global climate change itself, the solution to constraining climate projections will not be unique and should probably be thought as the agglomeration of many parallel techniques rather than the desperate search for a “magical” metric.

References :

Boé, J., and L. Terray (2014), Land-sea contrast, soil-atmosphere and cloud-temperature interactions: interplays and roles in future summer European climate change, Clim. Dyn., 42, 683-699, doi:10.1007/s00382-013-1868-8

Cattiaux, J., H. Douville, A. Ribes, F. Chauvin and C. Plante (2013) Towards a better understanding of wintertime cold extremes over Europe: a pilot study with CNRM and IPSL atmospheric models. Clim. Dyn., published online. doi: 10.1007/s00382-012-1436-7.

Cattiaux, J., H. Douville, Y. Peings (2013) European temperatures in CMIP5: origins of present-day biases and future uncertainties. Clim. Dyn., doi:10.1007/s00382-013-1731-y

Cattiaux, J., H. Douville, J. Najac, S. Parey, R. Schoetter, R. Vautard, P. Yiou (2014) Projected increase in the daily variability of European summer temperatures. Geophys. Res. Lett., submitted

Douville, H., I. Beau, J. Cattiaux, S. Tyteca (2014) Mid-latitude summer temperature biases and responses in CMIP5 models: the US Great Plain case study (in preparation)

Meehl, G. A., R. Moss, K. E. Taylor, V. Eyring, R. J. Stouffer, S. Bony, and B. Stevens, Climate Model Intercomparison: Preparing for the Next Phase, Eos, Trans. AGU, 95(9), 77, 2014.

Peings Y., J. Cattiaux, H. Douville (2012) Evaluation and response of cold spells over Western Europe in CMIP5 models. Clim. Dyn., doi:10.1007/s00382-012-1565-z

Schoetter R., J. Cattiaux, H. Douville (2014) Changes of western European heat wave characteristics projected by the CMIP5 ensemble. Clim. Dyn., in preparation

Seneviratne, S. et al. (2013) Impact of soil moisture-climate feedbacks on CMIP5 projections: First results from the GLACE-CMIP5 experiment. Geophys. Res. Lett., 40, 1–6, doi:10.1002/grl.50956

Stegehuis, A., R. Vautard, P. Ciais, A. Teuling, M. Jung, and P. Yiou (2013) Summer temperatures in Europe and land heat fluxes in observation-based data and regional climate model simulations. Clim. Dyn., 41, 455-477, doi:10.1007/s00382-012-1559-x

Vial, J., J-L. Dufresne, S. Bony (2013) On the interpretation of inter-model spread in CMIP5 climate sensitivity estimates. Clim. Dyn., 41, 3339–3362, doi:10.1007/s00382-013-1725-9